IMPACT OF CHANGING CLIMATE ON BROADBAND INFRASTRUCTURE IN MISSOURI

Fengpeng Sun, Ph.D., The University of Missouri–Kansas City

and

Patrick Market, Ph.D., The University of Missouri

IMPACT OF CHANGING CLIMATE ON BROADBAND INFRASTRUCTURE IN MISSOURI

ABSTRACT

Climate change is a significant threat to the environment and human society because it can increase the number of extreme weather and climate events and impact infrastructure. Researchers have been utilizing Atmosphere-Ocean General Circulation Models (AOGCMs) to predict future climate change. This study investigated the regional-scale climate change signals in Missouri at the end of the 21st century using AOGCMs projections from the Coupled Model Intercomparison Project's sixth phase (CMIP6). The projections used in this study were Historical and Shared Socioeconomic Pathway 5-8.5 (SSP5-8.5). The Historical projections represent the present-day climate. In contrast, the SSP5-8.5 projections represent climate at the end of the 21st century without attempts to reduce greenhouse gas emissions and mitigate climate change. We focused on two climate variables: precipitation and wind speed. Both long-term mean climate change and extremes of the two variables were explored. The study found that state-wide precipitation is expected to increase annually and for all seasons except summer. In contrast, the wind speed is projected to decrease annually and during all seasons. Further analysis of changes to the daily extreme precipitation and wind speed events was focused on the boreal winter and summer. Percentile-based thresholds were used to identify the days with extreme events. The analysis found that during the winter, there was an increase in the number of days with wet precipitation extremes while a decrease in the number of days with wind speed extremes. During the summer, there was a decrease in the number of days with wind speed extremes and a decrease in the number of

days with wet precipitation extremes. At the end of the century, Missouri's broadband infrastructure is projected to be at a greater risk of mean precipitation change and extreme precipitation events than wind speed changes.

CONTENTS

ILLUSTRATIONS

Figure Page

TABLES

Table Page

CHAPTER 1

BACKGROUND

1.1 Climate Change

Climate change is a critical threat to society because it affects the frequency of extreme events, which can significantly affect civil infrastructure. Climate change is largely a consequence of human activities. Humans have contributed to climate change by releasing substantial greenhouse gases (e.g., carbon dioxide, methane, nitrous oxide, etc.) into the atmosphere mainly through fossil fuel burning and land use practices. The increase in greenhouse gases allows more heat to be trapped in the lower atmosphere, increasing the planet's surface temperature (Schneider 1989). This effect is well known as the Greenhouse Effect. The increase in temperature affects Earth's natural systems. Earth's weather patterns and frequency of extreme weather events will change due to the temperature increase.

Climate change can result in wind speed and precipitation changes that negatively affect our environment. For instance, increasing temperatures can affect wind speed by affecting the pressure differences between air masses. Wind speed may increase or decrease depending on the area where the air masses meet. An increase in winds can result in stronger storms and potentially extreme weather events, such as tornados. The increased temperatures will also allow for an increase in the water vapor content in the air, likely leading to more extreme precipitation events in particular areas. These extreme precipitations can lead to catastrophic floods on the surface. Increased wind speeds and precipitation events would create massive environmental, infrastructural, and economic impacts. Therefore, research efforts are in place to assess, prepare and plan for the potential impacts of climate change.

1.2 Climate Modeling

Researchers are currently using global climate models as a major tool to project future environmental conditions, which will aid in identifying vulnerable areas so they can help plan and prepare to manage the climate change impact. Climate models project Earth's climate by simplifying the real world into mathematical equations representing physical, chemical, and biological principles and interactions (McGuffie and Henderson-Sellers 2014). There are many climate models available. Climate modeling has a long history beginning with conceptual models and currently with the Atmosphere-Ocean General Circulation Model (Edwards 2011). Atmosphere-Ocean General Circulation Models (AOGCMs) are known as coupled climate models because they connect atmospheric and oceanic models to help represent Earth's climate.

Researchers can use AOGCMs to examine past, present, and future climates. Researchers use these models by adjusting the initial conditions inputted into the climate model to project what the climate might look like under different scenarios. AOGCMs require a lot of computational power and time to run all necessary calculations. These models can output data about future temperature, precipitation, wind, and many other climatic variables. Researchers then analyze the output data to examine potential changes in future climate conditions. This information will be valuable in informing policymakers to make crucial decisions to adapt to and mitigate climate change.

Researchers have some confidence in these AOGCMs projections because AOGCMs are rigorously assessed by comparing model projections to observed records. AOGCMs simulations have shown large-scale aspects of climate similar to observed records; however, some exceptions have occurred (Raäisaänen 2007). AOGCMs are potent tools but have limitations primarily due to climate complexity and computational demand that hinder their results. AOGCMs can model many vital elements of Earth's climate, but there are many complex interactions and aspects of

climate that are not well enough understood or cannot be modeled with the current technology. These limitations make climate modeling challenging, but many groups are working to improve AOGCMs' complexity and computational power.

Due to the number and complexity of AOGCMS, collaborative efforts have formed to experiment, compare, or analyze these models. Two significant collaborative efforts focusing on climate change are the Coupled Model Intercomparison Project (CMIP) and the Intergovernmental Panel on Climate Change (IPCC). The World Climate Research Programme organizes CMIP, and its objective is to improve our understanding of past, current, and future climate change under different scenarios and contexts (O'Neill et al. 2016). CMIP focuses on experimenting and comparing coupled climate models from different climate modeling groups worldwide. There are more than twenty climate modeling groups participating in CMIP. CMIP has a structured approach to experiments that modeling groups must follow. After the modeling groups conduct their experiments, they can post their output to the Earth System Grid Federation (Meehl et al. 2014). The Earth System Grid Federation (ESGF) allows the research community to create an account and get access to the data. The data from CMIP is publicly available for the scientific community to analyze and compare. Data availability from CMIP has allowed the research community to analyze and compare results from various experiments. In this study, we downloaded the AOGCM output from the ESGF data portal, and stored and analyzed the data in our workstations.

Whereas the IPCC was established in 1988 by the World Meteorological Organization and the United Nations Environment Programme (Agrawala 1998). The IPCC's goal was to provide an analysis of climate change research to help create policy and improve our understanding (Bolin 2007). As a result, the IPCC has released many reports that detail analysis

of climate models, the impact of climate changes, and potential suggestions to improve our situation. The IPCC is divided into three working groups, each on different aspects of climate change. Countries worldwide work together in the IPCC to form these working groups. The results of their challenging work were published in the IPCC assessment reports. The IPCC has conducted many assessments over the years and has become a leader in disseminating the latest climate change information. These collaborative efforts are in place to help provide the most accurate and detailed information about the current climate change situation.

1.3 IPCC Projections

The IPCC recently released its sixth and most up-to-date assessment report detailing the latest information about the science of climate change, potential impacts, and mitigation efforts. The IPCC utilizes CMIP6 models in their reports and provides insight into the potential results that could occur in our study. The latest IPCC report provides information about how extreme winds and extreme precipitation might change due to climate change. The IPCC has observed a decline in extreme winds for the continental northern mid-latitudes. However, there is low confidence due to the small number of studies and uncertainties (Seneviratne et al. 2021). Extreme winds are under-explored compared to other climate variables and require greater research efforts to get a better understanding of what the future might look like. Precipitation, on the other hand, is a core climate variable that is explored much more than wind speed. The IPCC has high confidence that heavy precipitation will become more frequent at the global scale with additional warming; however, at regional scales, it will depend on warming, atmospheric circulation, and storm dynamics (Seneviratne et al. 2021). The changes in extreme precipitation may increase the likelihood of floods or droughts.

1.4 Missouri Background

Many studies that have utilized CMIP data typically focus on the global scale because climate change is a global issue. However, examining climate change at regional scales is also essential because climate change can vary drastically depending on location. Unfortunately, there is a lack of climate change research for regional locations such as Missouri. Missouri is located in the Midwest of the United States and is known for its agricultural prowess. Missouri has a population of approximately 6.1 million people and a total area of 69,000 square miles (Rafferty and Westermann 2023). Missouri has a medium size population and total area compared to the other states in the US. Missouri is also a landlocked state that has a continental type of climate. Missouri's climate is influenced by the cold air from Canada and warm air from the Gulf of Mexico (Rafferty and Westermann 2023). The air masses reach Missouri easily to form wind because there are no barriers like mountains to interfere with the path of the air masses. Missouri has strong seasonal climate characteristics. During the winter months, Missouri's temperatures are cold, with low precipitation. However, during the summer months, Missouri's temperatures are hot, with high precipitation. Due to its climate, natural disasters that can occur in Missouri are floods, droughts, tornadoes, and severe storms, which have influential impacts on infrastructures. These natural disasters may increase in frequency due to climate change. Quantifying climate change in Missouri can help examine, plan, and prepare for future climate change impacts.

1.5 Objectives

Our study aimed to explore the potential changes in two climate variables: precipitation and wind speed in Missouri toward the end of the 21st century by utilizing Atmosphere-Ocean General Circulation Models (AOGCMs) from CMIP's sixth phase. Analyzing these two variables is essential to understand the potential vulnerability and resiliency of the state's

broadband infrastructure to future regional climate change. The study had two primary objectives to achieve this aim. The first objective investigated the long-term climatological mean changes in wind speed and precipitation. The second objective evaluated the frequency of extreme wind speed and precipitation events during the winter and summer seasons. The AOGCMs from CMIP provided Historical and SSP5-8.5 experiment scenario data that were analyzed to achieve the two objectives. These objectives provided valuable insight into the potential changes that could occur in the future and how they could potentially affect broadband infrastructure.

CHAPTER 2

METHODOLOGY

2.1 CMIP6 Projections

We collected CMIP6 AOGCMs' average surface wind speed (sfcwind) and precipitation flux (PR) output data from the Earth System Grid Federation data archive website (ESGF). The ESGF allows us to download a wide range of experimental data. The experimental data utilized in our study was Historical and SSP5-8.5. According to Erying et al. (2016), the Historical experiment simulates past climate spanning from 1850 to 2014. They also detail how historical data can be used to evaluate climate model performance because they can compare their results to instrument measurements from 1850 to the present. However, our study used Historical data only to obtain simulated past precipitation and wind speed values. The SSP5-8.5 experiment simulates future climate based on SSP5 and RCP 8.5 scenarios (O'Neill et al. 2016). The SSP5-8.5 experiment data spans from 2014 to 2100 and is considered the worst-case scenario where there is no attempt to reduce carbon emissions to mitigate climate change. Therefore, our study used the Historical data as the baseline and the SSP5-8.5 data as the future for precipitation and wind speed.

The ESGF also provided access to many different institutions' AOGCM. These AOGCMs can output data at different frequencies and have different availabilities. The primary frequencies that our study used were monthly and daily. We used 29 different AOGCMs for wind speed. All 29 AOGCMs had monthly-mean data, while only 18 out of 29 had daily-mean data. For precipitation, we used 25 different available AOGCMs. All 25 AOGCMs had monthly data, while only 19 out of 25 had daily data. The monthly and daily AOGCM data had four data sets: Historical wind speed, SSP5-8.5 wind speed, Historical precipitation, and SSP5-8.5

precipitation. A summary of all the AOGCMs we used in our study can be found in Table 1 and Table 2. The monthly dataset explored the mean wind speed and precipitation changes. In contrast, the daily dataset was used to investigate the change in extreme wind speed and precipitation events.

Table 1. The information about all the CMIP6 models used for wind speed in the study.

Number	Institution	Country	Model	Grid (lat x lon)	Monthly Available	Daily Available
1	CSIRO-ARCCSS	Australia	ACCESS-CM2	144x192	✓	✓
2	CSIRO	Australia	ACCESS-ESM1-5	145x192	✓	✓
3	AWI	Germany	AWI-CM-1-1-MR	192x384	✓	
4	BCC	China	BCC-CSM2-MR	160x320	✓	
5	CAS	China	CAS-ESM2-0	128x256	✓	
6	CMCC	Italy	CMCC-CM2-SR5	192x288	✓	✓
7	CMCC	Italy	CMCC-ESM2	192x288	✓	✓
8	CNRM-CERFACS	France	CNRM-CM6-1	128x256	✓	
9	CNRM-CERFACS	France	CNRM-CM6-1-HR	360x720	✓	
10	CNRM-CERFACS	France	CNRM-ESM2-1	128x256	✓	
11	CCCma	Canada	CanESM5	64x128	✓	✓
12	EC-Earth-Consortium	European	EC-Earth3	256x512	✓	✓
13	CAS	China	FGOALS-f3-L	180x288	✓	
14	NOAA-GFDL	USA	GFDL-ESM4	180x288	✓	✓
15	NASA-GISS	USA	GISS-E2-1-G	90x144	✓	
16	NASA-GISS	USA	GISS-E2-1-H	90x144	✓	
17	NASA-GISS	USA	GISS-E2-2-G	90x144	✓	
18	MOHC	UK	HadGEM3-GC31-LL	144x192	✓	✓
19	MOHC	UK	HadGEM3-GC31-MM	324x432	✓	✓
20	INM	Russia	INM-CM4-8	120x180	✓	✓
21	INM	Russia	INM-CM5-0	120x180	✓	✓
22	IPSL	France	IPSL-CM6A-LR	143x144	✓	✓
23	NIMS-KMA	Republic of Korea	KACE-1-0-G	144x192	✓	
24	MIROC	Japan	MIROC-ES2L	64x128	✓	✓
25	MIROC	Japan	MIROC6	128x256	✓	✓
26	MPI-M	Germany	MPI-ESM1-2-HR	192x384	✓	✓
27	MPI-M	Germany	MPI-ESM1-2-LR	96x192	✓	✓
28	MRI	Japan	MRI-ESM2-0	160x320	✓	✓
29	MOHC	UK	UKESM1-0-LL	144x192	✓	✓

Table 2. The information about all the CMIP6 models used for precipitation in the study.

Number	Institution	Country	Model	Grid (lat x lon)	Monthly Available	Daily Available
1	NCAR	USA	CESM2-WACCM	192x288	✓	✓
2	NASA-GISS	USA	GISS-E2-1-G	90x144	✓	
3	BCC	China	BCC-CSM2-MR	160x320	✓	✓
4	AS-RCEC	Taiwan	TaiESM1	192x288	✓	✓
5	UA	USA	MCM-UA-1-0	80x96	✓	
6	CAS	China	FGOALS-f3-L	180x288	✓	
7	CCCma	Canada	CanESM5	64x128	✓	✓
8	CMCC	Italy	CMCC-CM2-SR5	192x288	✓	✓
9	CSIRO	Australia	ACCESS-ESM1-5	145x192	✓	✓
10	FIO-QLNM	China	FIO-ESM-2-0	192x288	✓	
11	INM	Russia	INM-CM4-8	120x180	✓	✓
12	IPSL	France	IPSL-CM6A-LR	143x144	✓	✓
13	KIOST	Republic of Korea	KIOST-ESM	96x192	✓	✓
14	MIROC	Japan	MIROC6	128x256	✓	✓
15	MOHC	UK	UKESM1-0-LL	144x192	✓	✓
16	MRI	Japan	MRI-ESM2-0	160x320	✓	✓
17	NIMS-KMA	Republic of Korea	KACE-1-0-G	144x192	✓	✓
18	NOAA-GFDL	USA	GFDL-ESM4	180x288	✓	✓
19	NUIST	China	NESM3	96x192	✓	✓
20	THU	China	CIESM	192x288	✓	
21	CSIRO-ARCCSS	Australia	ACCESS-CM2	144x192	✓	✓
22	CNRM-CERFACS	France	CNRM-ESM2-1	128x256	✓	✓
23	E3SM	USA	E3SM-1-1	180x360	✓	
24	MPI-M	Germany	MPI-ESM1-2-LR	96x192	✓	✓
25	NCC	Norway	NorESM2-LM	96x144	✓	✓

After collecting all the model output data, we needed to preprocess it into a usable form for analysis and comparison because the data sets have different grid sizes, daily frequency outputs, and suboptimal units. The models used in our study had a wide range of grid sizes because each model outputs data differently. The grid size differences are an issue because it affects the resolution of the data. Therefore, we used MATLAB to create a standard grid cell size for all the models. All the models were linearly interpolated to a standard common grid cell size of 1 degree by 1 degree. The other issue we had was the daily model frequency output because

some models included leap year days, did not include leap, or decided to have 30 days every month. The most common daily frequency output did not include leap years which is 365 days for all years. Only a few models included leap years or had 30 days for all the months. We chose to adjust all the datasets to 365 days per year because this would require the least modification of the data sets. If a dataset included leap years, the additional day, i.e., February 29th was removed, and if the dataset had 30 days for all the months, the 31st day was calculated by taking the average between the months. Lastly, the original data sets had kg m^{-2} s^{-1} as the unit for precipitation. The precipitation data sets were converted to mm per day because these units are more common when describing precipitation.

2.2 Area of Interest

Missouri is the area of interest of our study. Figure 1 shows the map of the Missouri region with state boundary outlined. The exact location of the Missouri region used in our study was 35.5 to 41.5 degrees latitude and -96.5 to 88.5 degrees longitude. The study area contains 6 degrees latitude and 8 degrees longitude. Our study area provided 48 grid data sample points from each model since the cell size for each model is interpolated to 1 degree by 1 degree. The Historical data focused on the 1984-2014 period for this location, and the SSP5-8.5 data focused on the 2070 to 2100 period. The study period is 31 years long because it is a long enough period to reflect long-term climatology. We first investigated the mean annual and seasonal wind speed and precipitation change. Then we investigated extreme wind speed and precipitation extremes for all seasons during the study periods, and our results on extremes focused on the summer and winter seasons. The seasons were divided into three-month groups. Winter was December, January, and February (DJF). Then spring was March, April, and May (MAM). Next, the summer was June, July, and August (JJA). Lastly, fall was September, October, and November

(SON). For the winter season, the previous year's December was used to calculate the winter season's average.

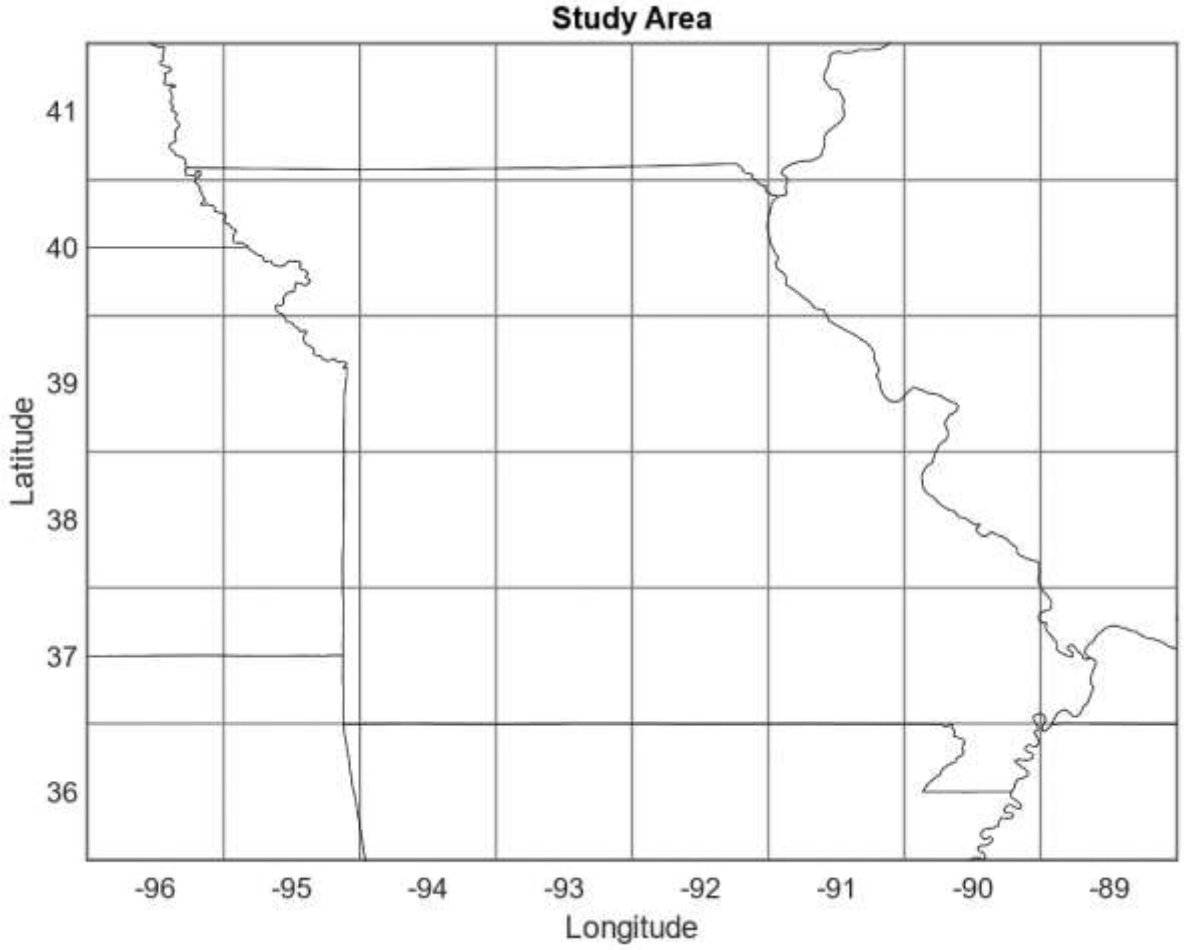

Figure 1. Missouri study area for mean climate change and extreme climate change analysis.

2.3 Mean Climate Change

2.3.1 Wind Speed Change

The wind speed change analysis investigated annual and seasonal changes. The data used in this analysis were monthly Historical and SSP5-8.5 wind speed data from all 29 AOGCMs in Table 1. The annual wind speed changes analysis was calculated using all 12 months, and the seasonal wind speed changes analysis was calculated by dividing each data set into 3-month

groups. Five main calculations were conducted on both the annual and seasonal data. The first calculation averaged every grid cell for all 29 models' Historical and SSP5-8.5 wind speed data for the target location and period. Averaging all the grid cells provides 48 mean wind speed values for the Historical and SSP5-8.5 wind speed data. The second calculation subtracted each model's SSP5-8.5 mean wind speeds with the corresponding Historical mean wind speeds. The subtraction resulted in the mean wind speed change for each model. The third calculation averaged all the models into one mean wind speed change. The third calculation examines the wind speed change based on all models. The fourth calculation focused on calculating the area mean of the mean wind speed change for all the models. The area means averaged each model's 48 mean wind speed change grid cells. The area means provided a single value to represent each model. The last calculations were descriptive statistics on the area means. Descriptive statistics help describe the annual and seasonal mean wind speed changes.

2.3.2 Precipitation Change

The precipitation change analysis also explored annual and seasonal changes. The data used in the precipitation analysis were monthly Historical and SSP5-8.5 precipitation data from all 25 AOGCMs in Table 2. The precipitation change analysis calculations are almost identical to the wind speed change analysis. The main difference is the method to measure mean change. The first calculation was averaging every grid cell for all 25 models' Historical and SSP5-8.5 precipitation data. The second calculation is where things are different. The wind speed analysis method measured mean wind speed change by calculating the difference between each model's SSP5-8.5 and Historical mean wind speeds. In contrast, the precipitation analysis measured mean precipitation change by calculating the percentage change between each model's Historical and SSP5-8.5 mean annual and seasonal precipitation. Percent change was chosen over calculating

the difference because it is easier to interpret the results and is a common practice in precipitation change studies. For example, if the result showed a 3 mm per day increase, it is hard to tell if that is a big or small increase, but if the result was a 60 percent increase, it is much easier to understand quantitatively. The third calculation averaged all the models into one mean precipitation percent change. The fourth calculation focused on calculating the area mean of the mean precipitation percent change for all the models. The last calculations were descriptive statistics on the area means.

2.3.3 Mean Change

The annual and seasonal wind speed and precipitation change analysis results were evaluated using maps, bar charts, tables, and heat maps. First, the mean wind speed and precipitation change results were plotted as maps. The maps were handy because they detailed the spatial variation of the mean wind speed and precipitation results for each model. Next, bar charts were created to examine the area means of the mean wind speed and precipitation results. The bar charts helped identify patterns and compare the models' results. Then, the descriptive statistics were calculated for the area means and organized into tables to make them easy to interpret. Lastly, heat maps were created to summarize the results of the annual and seasonal area means for wind speed and precipitation. The heat maps used colors adapted from Brewer and Harrower's color (2003) website to show the relationship between each model and the wind speed or precipitation change. All of the evaluation methods were also conducted with MATLAB.

2.4 Extreme Climate Change

2.4.1 Climate Extreme Indices

Many indices are available to investigate the frequency of wind speed and precipitation extremes. Most indices used either a fixed or percentile-based threshold to identify extremes. Fixed thresholds are subjective because they depend on the location. Zhang et al. (2011) provide an excellent example of how a 0º Celsius fixed threshold would indicate extreme cold during the winter for the mid-latitudes. However, it would not be suitable for higher latitudes because 0º Celsius be mild for higher latitudes regions. Conversely, percentile-based thresholds are more objective than fixed thresholds because they are calculated based on probability. Our study used percentile-based thresholds to quantify wind speed and precipitation extremes for the winter and summer seasons. We performed analysis for all seasons, while our study only focused on the winter and summer seasons because extremes are typically more impactful during these seasons than the transition fall and spring seasons. The indices used for winter and summer wind speed and precipitation extremes were a 95th percentile threshold.

2.4.2 Wind Speed and Precipitation Extremes

The wind speed and precipitation extremes both utilized percentile-based thresholds. The extreme wind speed calculation used daily-mean Historical and SSP5-8.5 data from 18 AOGCMs in Table 1. While the precipitation extreme calculations used daily-accumulated Historical and SSP5-8.5 data from 19 AOGCMs from Table 2. Both wind speed and precipitation adopted a 95th percentile threshold separately. Our study used percentile-based thresholds by first calculating the unique and individual threshold values for each grid cell for each of the models. The unique threshold values were calculated by sorting each Historical data set from least to greatest and selecting the wind speed or precipitation values based on the percentile for each grid cell. This calculation provided the unique threshold values and the corresponding number of days exceeded during the Historical period. Next, the unique threshold

values were used to calculate how many days were exceeded during the future SSP5-8.5 period. Then the number of days exceeded during the Historical period was subtracted from the number of days exceeded during the SSP5-8.5 period. Lastly, the number of days difference was divided by 31 to get the average days per year change.

The winter and summer wind speed and precipitation extremes were evaluated using maps. Multiple maps were created using custom color ramps based on Brewer and Harrower's (2003) website for the percentile-based thresholds. It’s noteworthy that their color schemes were adopted in the IPCC climate change assessment report. The maps described the changes in the number of extreme events for each grid cell and the spatial variation for the study area. Each percentile-based threshold had three maps: one for the unique threshold values, the difference between SSP5-8.5 and Historical, and the ensemble-mean difference.

CHAPTER 3

RESULTS: MEAN CHANGE

3.1 Wind Speed Change

3.1.1 Annual and Seasonal Change

The wind speed change analysis focused on annual and seasonal wind speed changes. A total of 29 AOGCMs were examined for the wind speed change analysis. Each model calculated a mean wind speed difference between SSP5-8.5 and Historical monthly wind speed data to determine annual and seasonal wind speed change. All 29 model results were averaged together to examine the GCM ensemble-mean annual and seasonal wind speed change. The results were then plotted into maps to examine the spatial variation and wind speed change values.

The ensemble-mean annual wind speed change in Figure 2 showed a general decrease in wind speed across the entire study area. The wind speed decrease was approximately 0.4 meters per second and displayed a pattern of decreasing wind speeds from the southwest to the northeast. The 29 models' annual wind speed changes used for the mean change are illustrated in Figure 3. Most models showed a decrease in wind speed for the entire study area; however, some models showed a mix of increasing and decreasing wind speeds. For example, models 9 and 13 had increases in wind speed in the west and a decrease in speed in the east, while model 8 shows an increase in nearly the whole region except the northeast corner.

Figure 4 displays the ensemble-mean seasonal wind speed changes. The mean wind speed change for all seasons shows mostly a decrease in wind speeds. Spring and summer seasons had very similar values and patterns in changes. Spring and summer seasons had an increase in wind speed in the southwest and a decrease in wind speed for the rest of the area, while winter and fall seasons showed only a decrease in wind speed for the entire area. A pattern

observed across all seasons is a more significant wind speed decrease in the northern part of the study region. The individual models' seasonal wind speed change was presented in Figures 5-8. Each season had model results that showed a wide variety of wind speed decreases and increases. During the winter, spring, and summer seasons, the models show mixed results because some models show increases in wind speed while others show decreases in wind speed. Spring and summer had a larger number of models with increases in wind speed than winter. For the fall, most models show a decrease in wind speed, and very few models show an increase in wind speed.

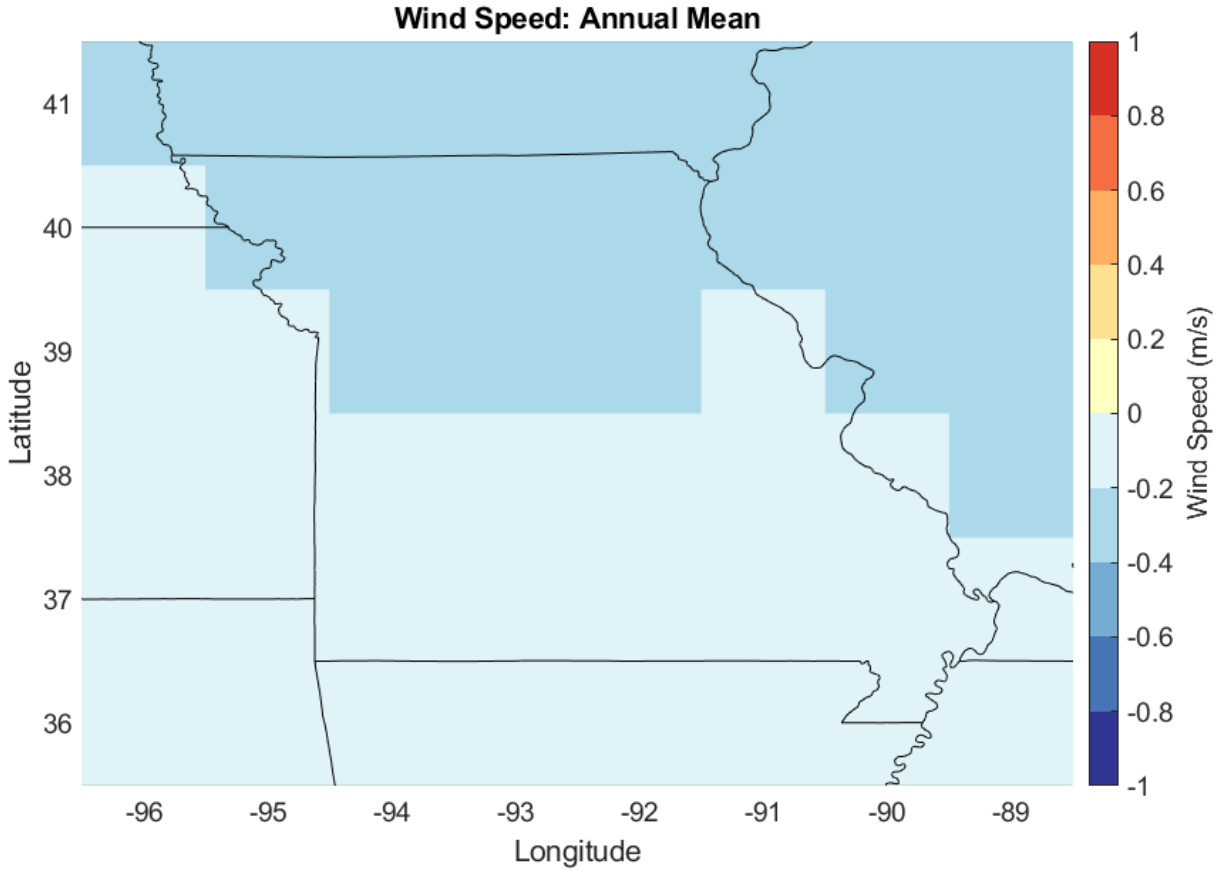

Figure 2. Mean annual wind speed change between SSP5-8.5 and Historical data for each grid cell. 29 models result were used for the mean.

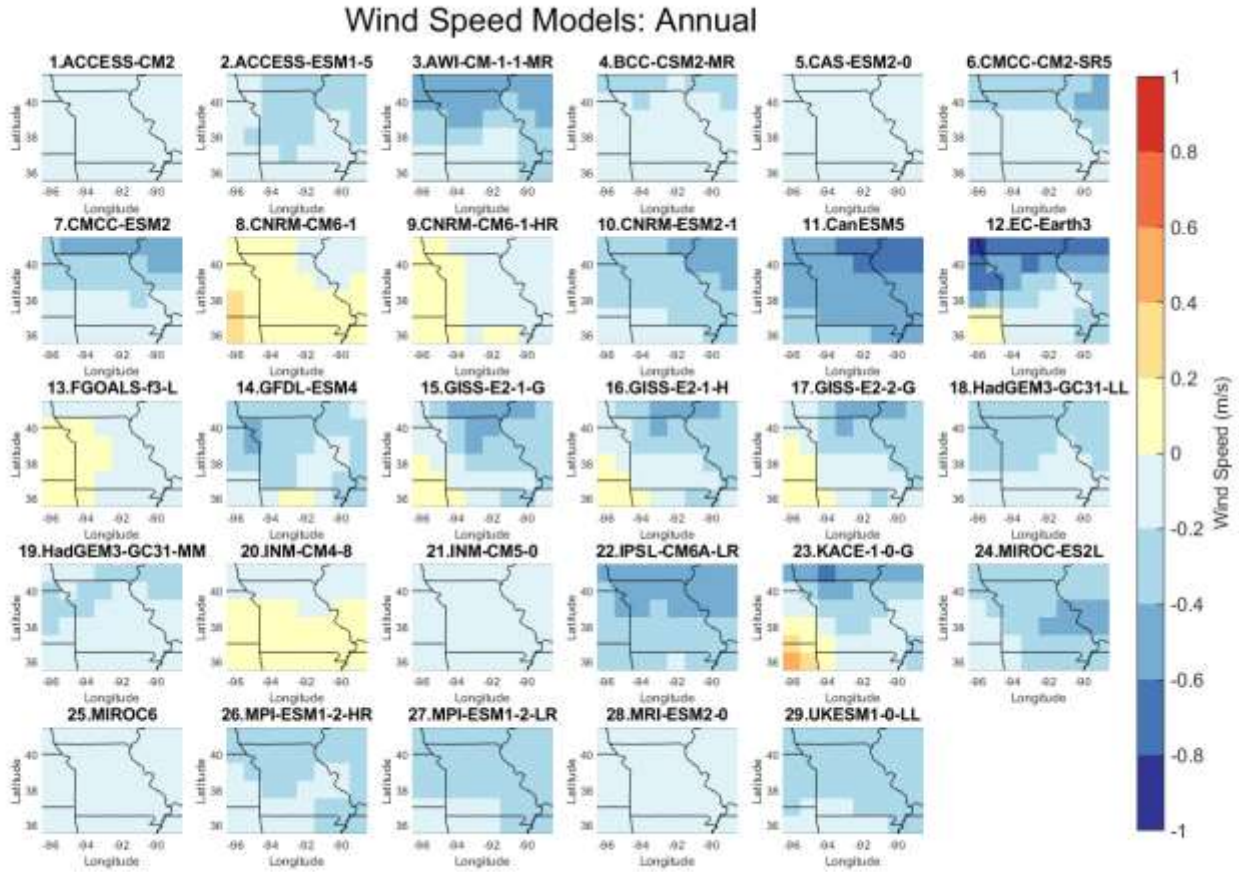

Figure 3. Annual wind speed difference between SSP5-8.5 and Historical for 29 models.

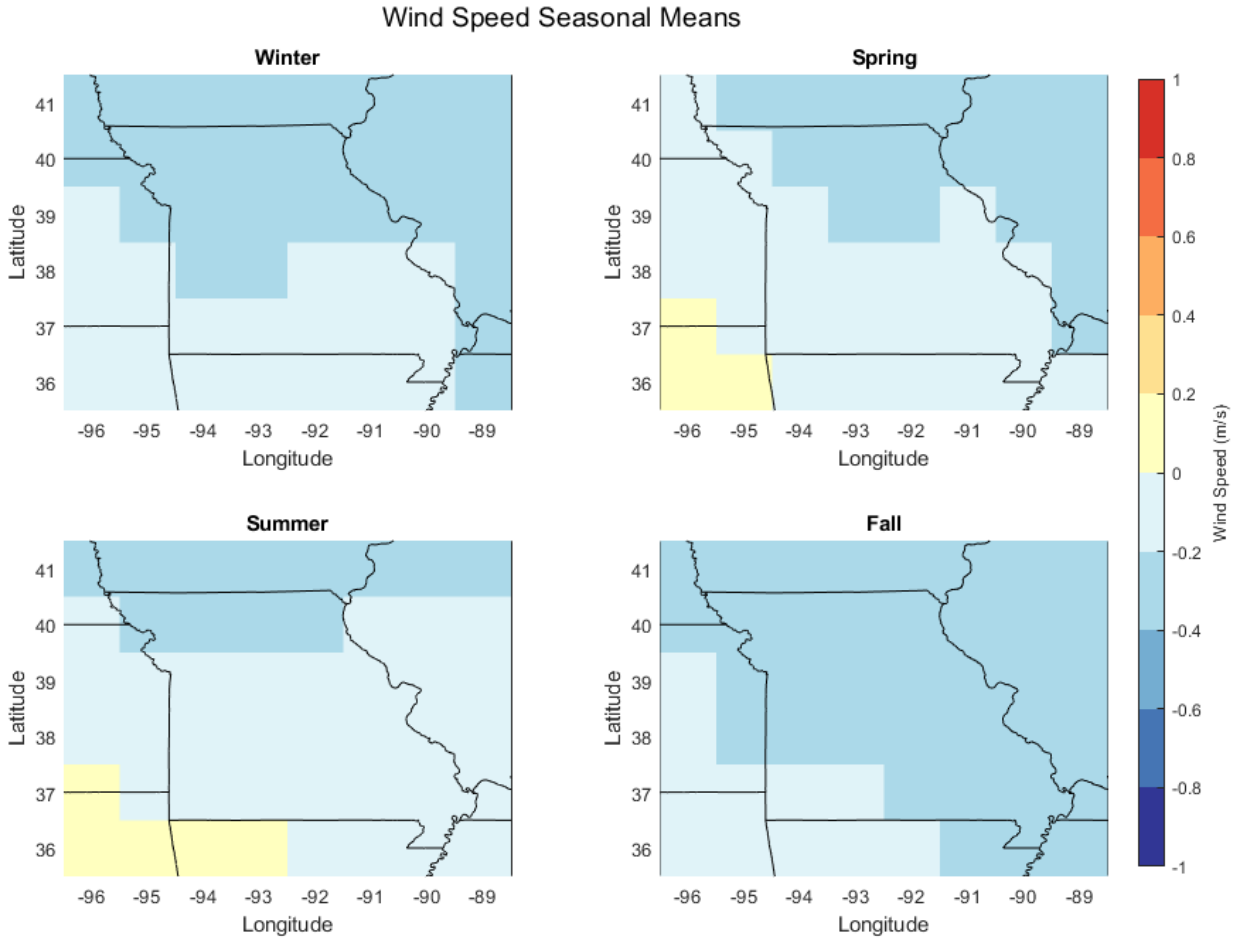

Figure 4. Mean seasonal wind speed difference between SSP5-8.5 and Historical for each grid cell.

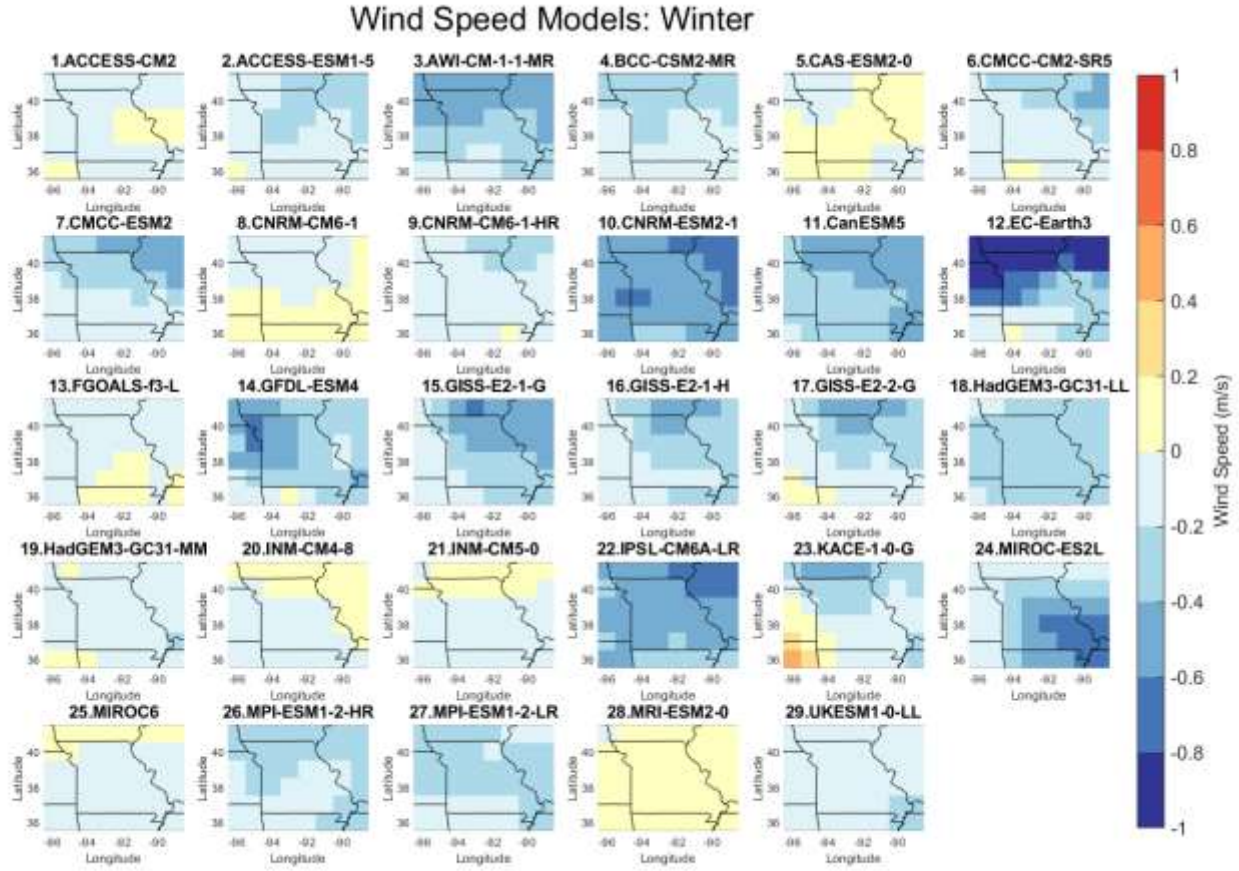

Figure 5. Mean winter wind speed difference between SSP5-8.5 and Historical for each model.

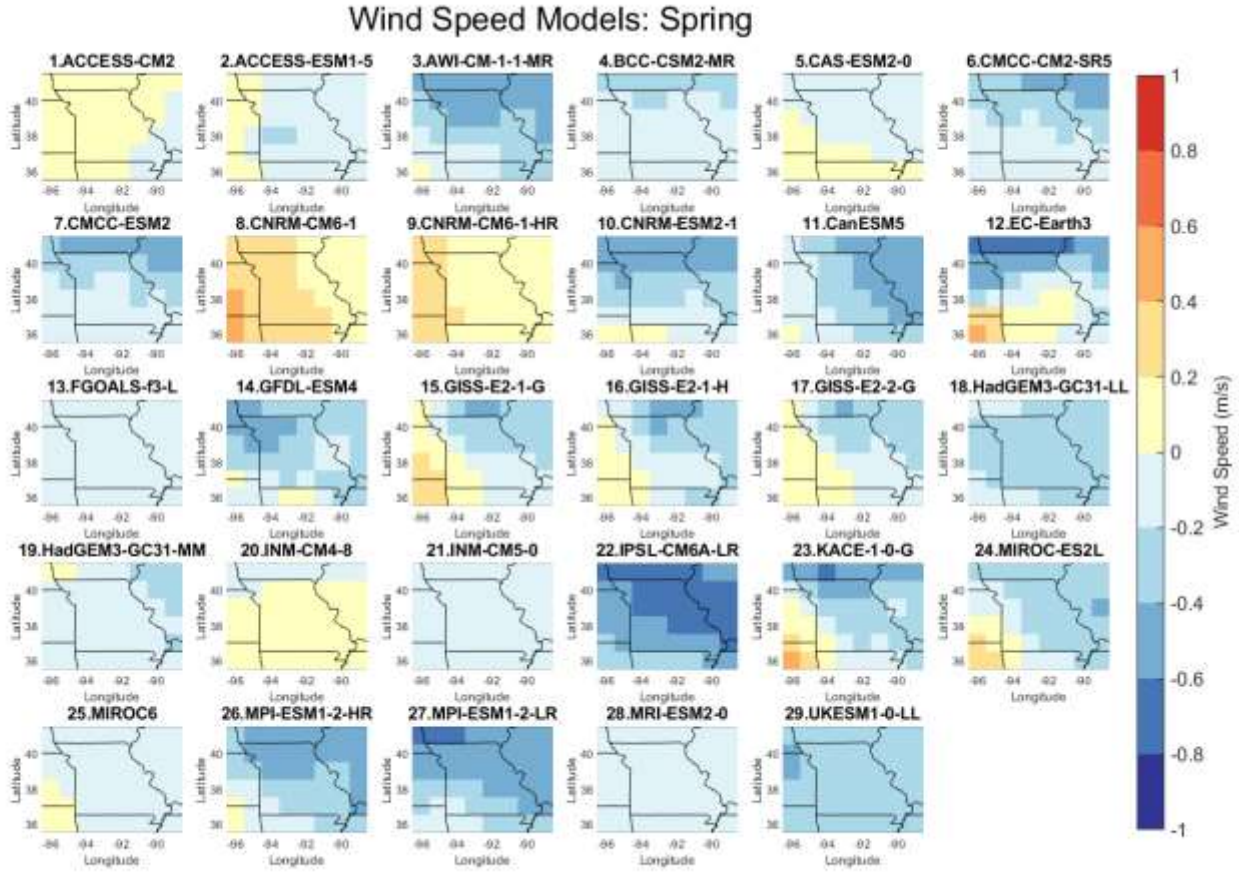

Figure 6. Mean spring wind speed difference between SSP5-8.5 and Historical for each model.

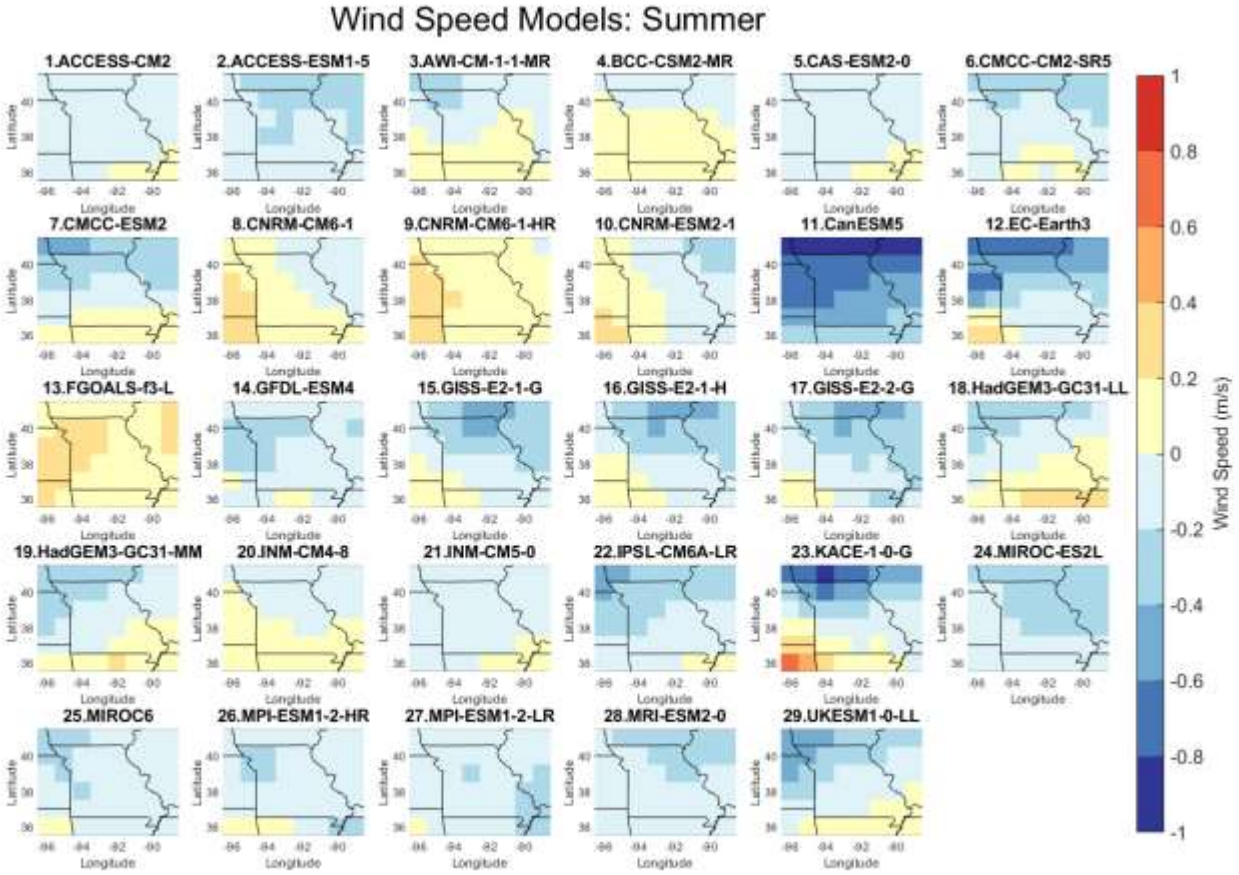

Figure 7. Mean summer wind speed difference between SSP5-8.5 and Historical for each model.

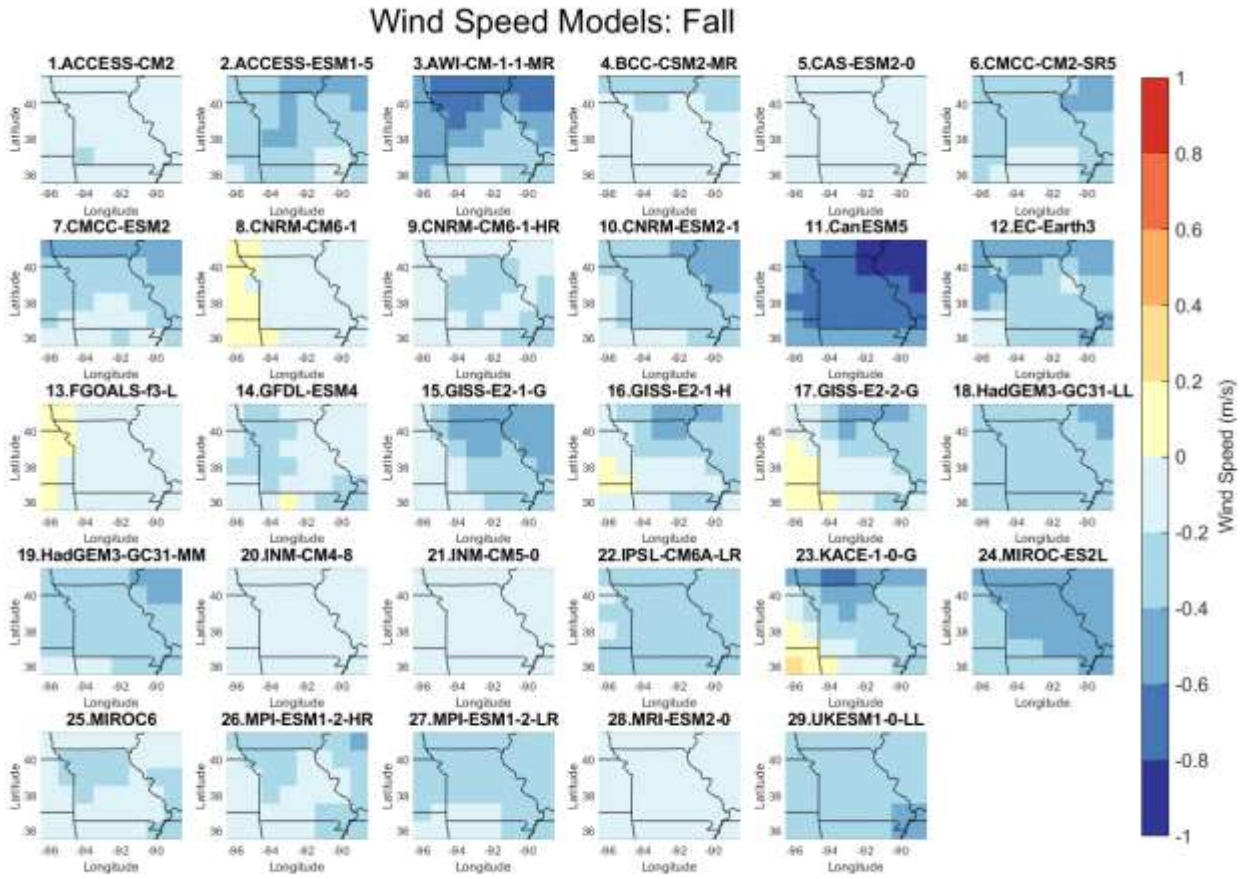

Figure 8. Mean fall wind speed difference between SSP5-8.5 and Historical for each model.

3.1.2 Area Mean Evaluation

An area mean across Missouri was calculated by averaging the wind speed change values from each model's grid cells. Area means were calculated for both the annual and seasonal wind speed changes. The area means analysis provides a different perspective on wind speed changes because one value can represent each model. The single value help quantify the changes observed from the maps. The annual and seasonal area means were presented as bar charts in Figure 9 and Figure 10. The annual and seasonal bar charts mostly showed a wide range of negative and reduced wind speeds. Descriptive statistics were calculated from the area means to understand the results better. The mean, median, standard deviation, maximum, minimum, and range can be found in Table 3. The information can be used to compare each season. Notable results were that winter had the smallest range, spring had the largest maximum, and fall had the largest minimum.

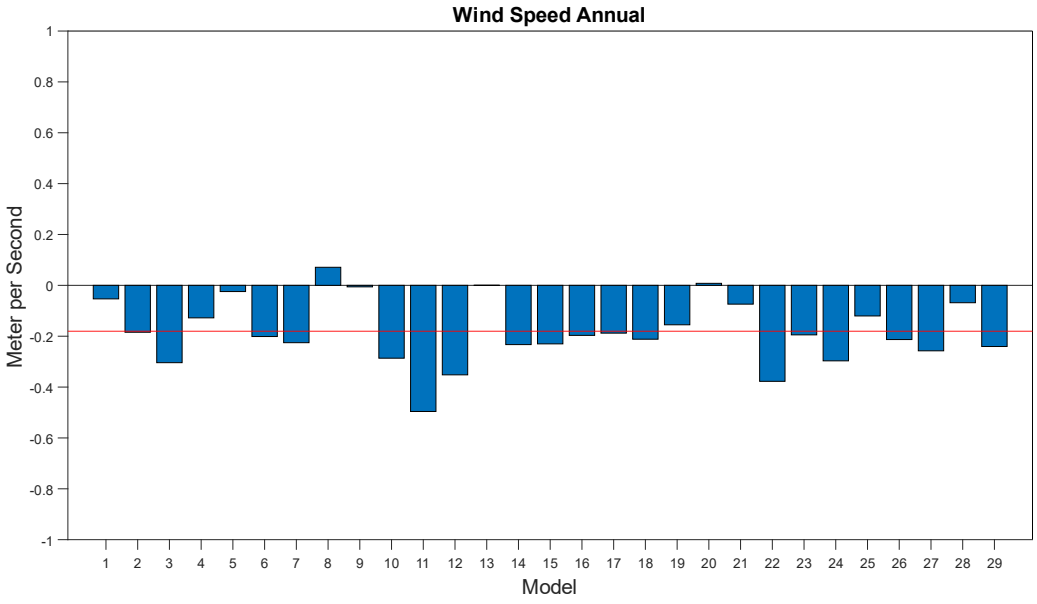

Figure 9. Area annual mean wind speed difference of each model. The red line is the ensemble mean of all the models.

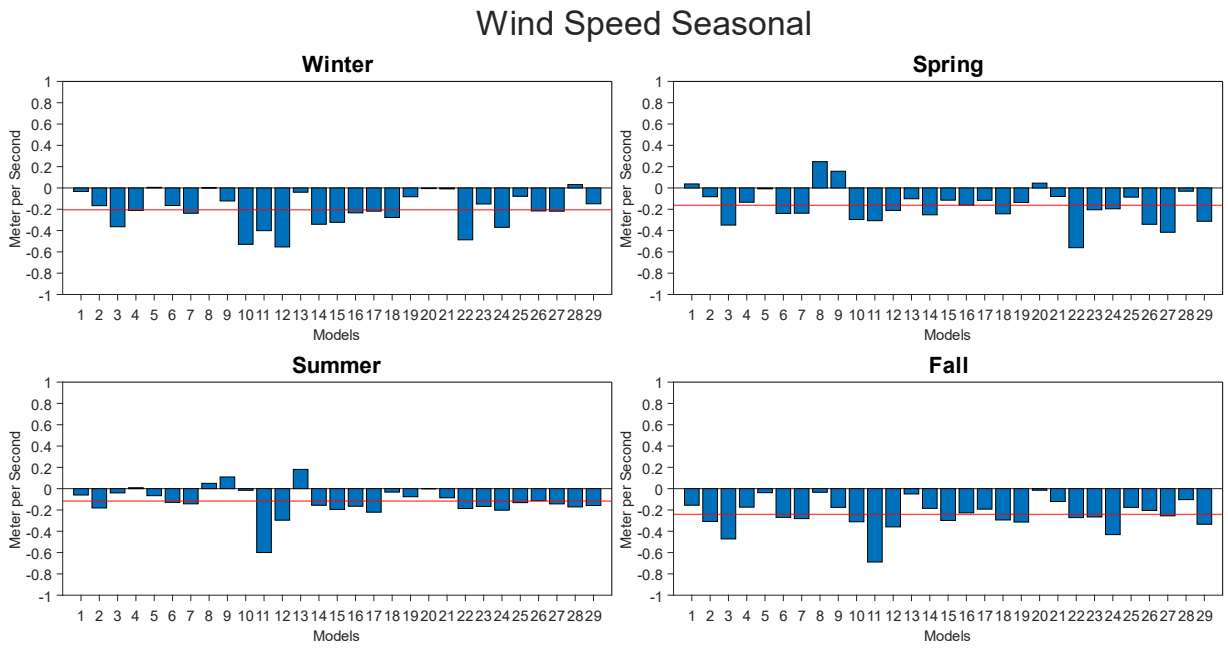

Figure 10. Area seasonal mean wind speed difference of each model. The red line is the mean of all the models.

Table 3. Descriptive statistics from the area mean wind speed change of all models.

	Winter	Spring	Summer	Fall	Annual
Mean	-0.20	-0.16	-0.12	-0.24	-0.18
Median	-0.21	-0.16	-0.13	-0.26	-0.20
Standard Deviation	0.16	0.17	0.14	0.14	0.13
Maximum	0.03	0.25	0.18	-0.02	0.07
Minimum	-0.55	-0.56	-0.60	-0.69	-0.50
Range	0.59	0.81	0.78	0.67	0.57

3.2 Precipitation Change

3.2.1 Annual and Seasonal Percent Change

Annual and seasonal mean precipitation percent change was the center of the precipitation change analysis. The precipitation change analysis utilized 25 AOGCMs. The mean percentage change was calculated between SSP5-8.5 and Historical monthly precipitation data from each model. Like the wind speed change analysis, the models were averaged to find the mean annual and seasonal precipitation percentage change. The results were also plotted into maps to examine the spatial variation and precipitation percent change values.

Figure 11 details the spatial pattern of the ensemble-mean annual precipitation percent change. The mean annual precipitation percent change is positive across the entire study area, indicating a generally wetter future. There is a southwest to northeast percent change increase. The most significant percent change increase was approximately 14 percent, and the smallest percent change increase was approximately 3 percent. The 25 models' annual precipitation percent change are displayed in Figure 12. Over half of the models had a positive percent change increase across the entire study area. However, a few models describe areas with negative percent change, such as model 6, indicating a drier future condition. The largest negative percent change is around 10 percent, while the largest positive percent change is close to 30 percent.

The ensemble-mean seasonal precipitation percent change is presented in Figure 13. The winter and spring season had all positive percent change, while summer had a mix of high negative and low positive percent change. Fall had low positive and negative percent change. The distribution patterns of low and high percent change are slightly different for each season. Figures 14-17 illustrate the 25 models' seasonal precipitation percent change. Most models during the winter and spring season had a positive percent change. A few models had a substantial positive percent change. The summer season, on the hand, had many models with

negative percent change. Lastly, the models in the fall season had a mix of light positive and negative percent change.

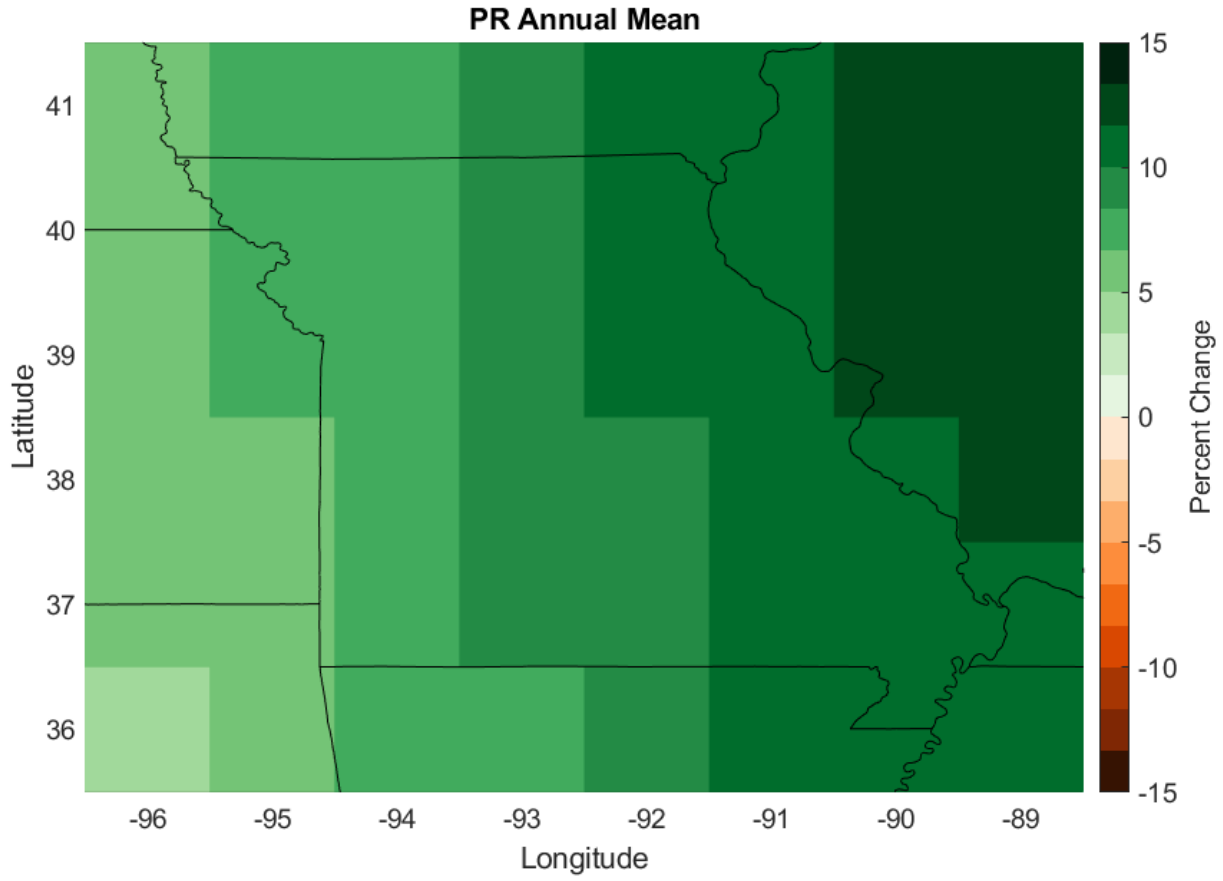

Figure 11. Mean annual precipitation percent change between SSP5-8.5 and Historical for each grid cell.

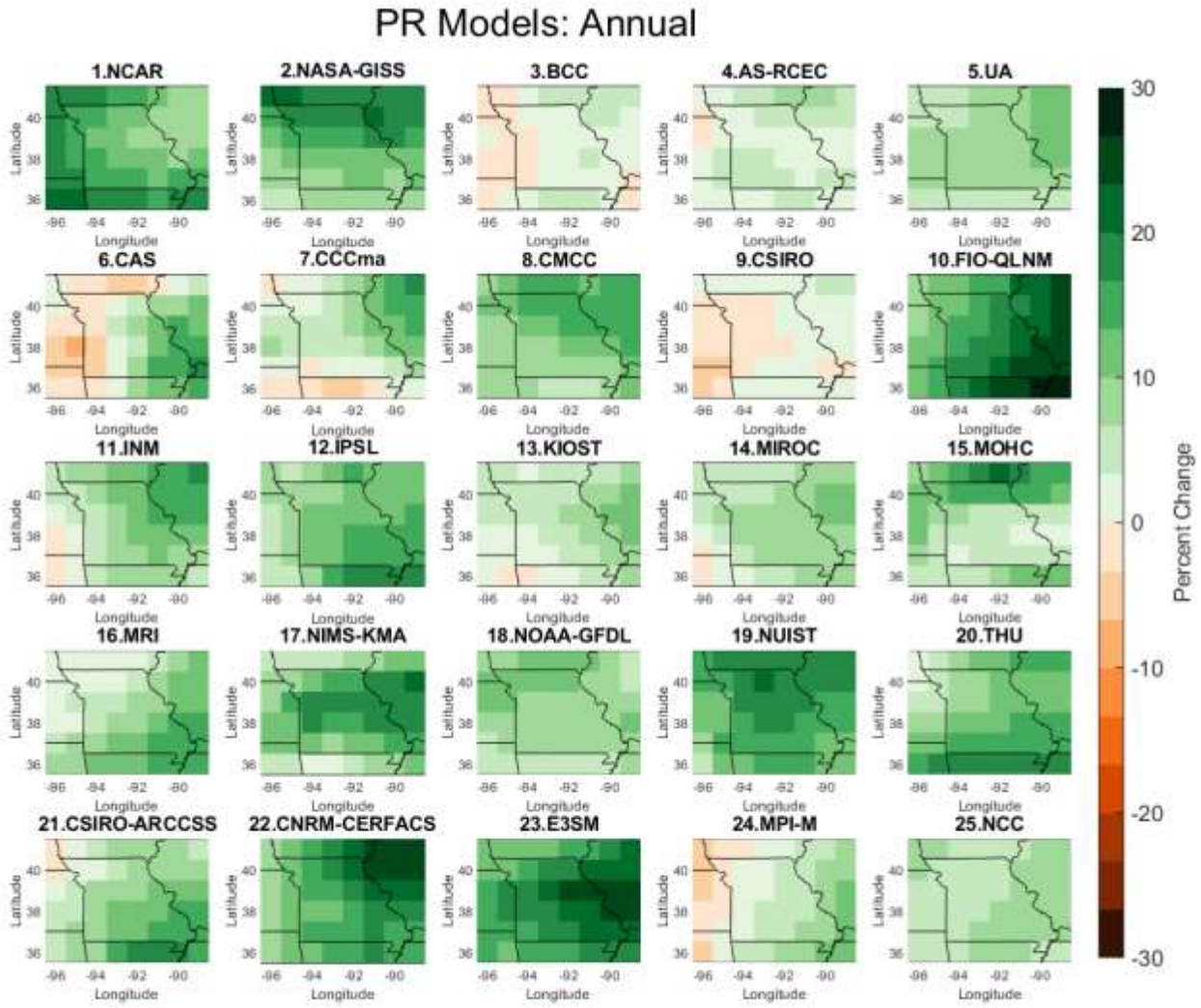

Figure 12. Mean annual precipitation precent change between SSP5-8.5 and Historical for each model.

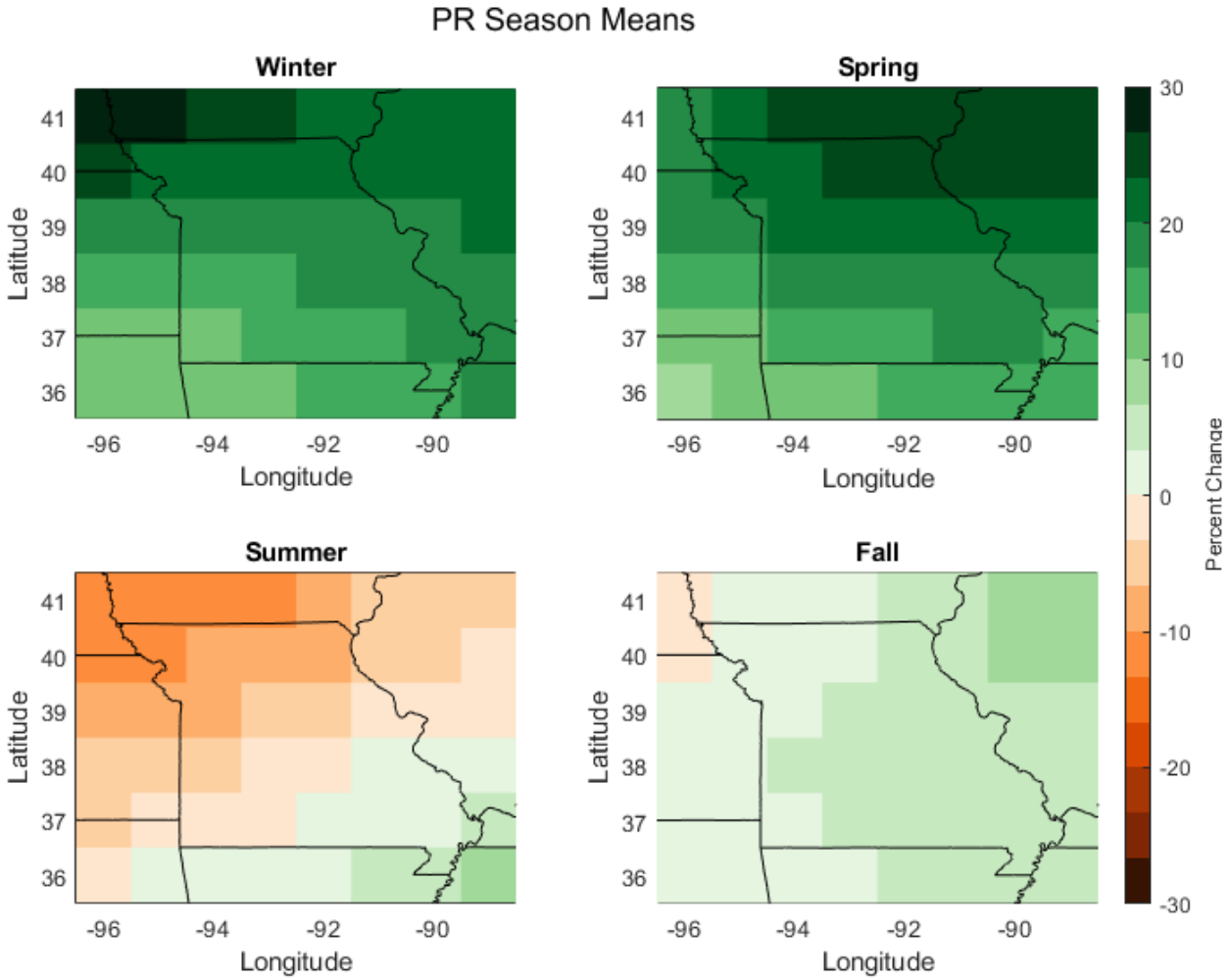

Figure 13. Mean seasonal precipitation precent change between SSP5-8.5 and Historical for each grid cell.

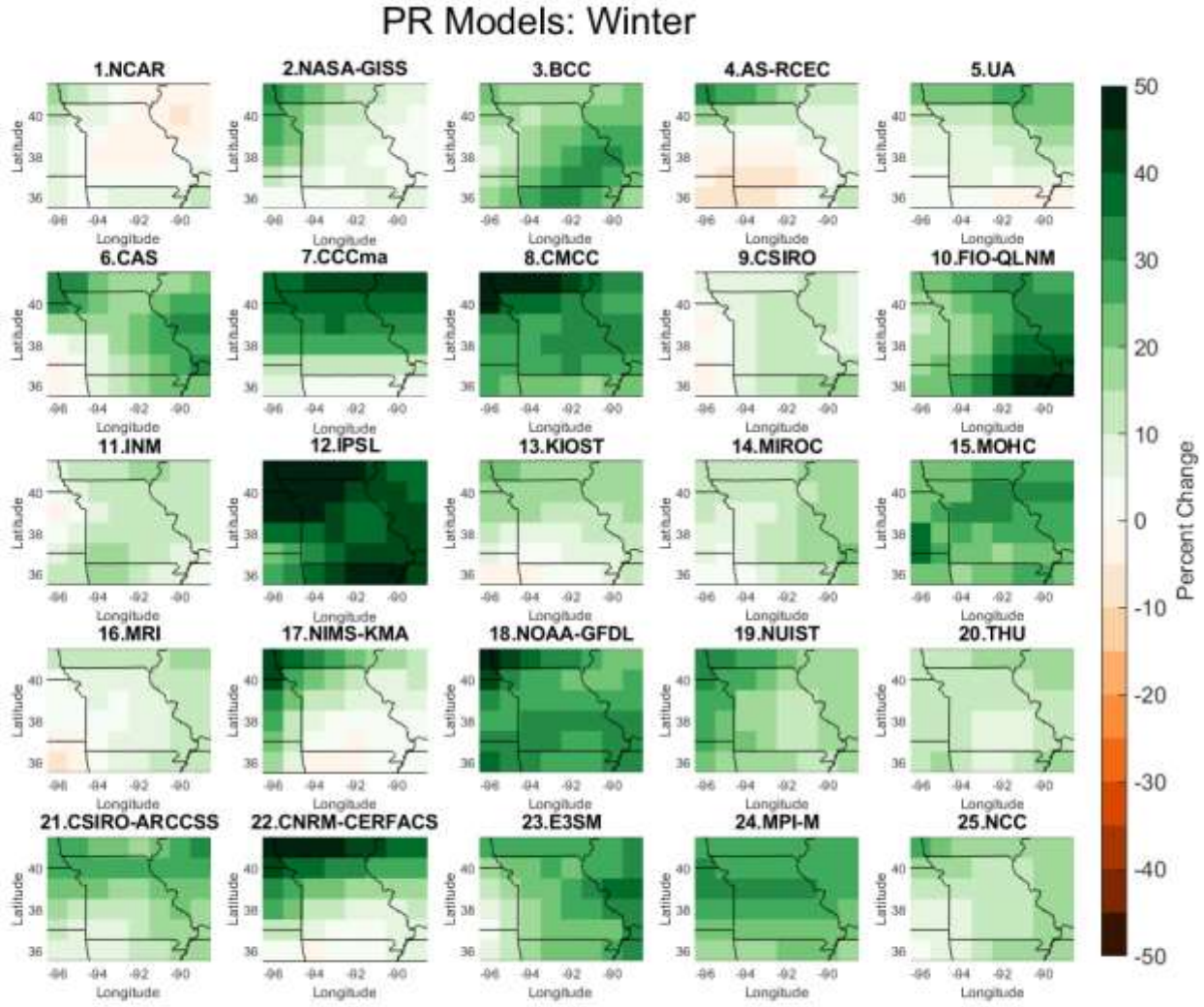

Figure 14. Mean winter precipitation precent change between SSP5-8.5 and Historical for each model.

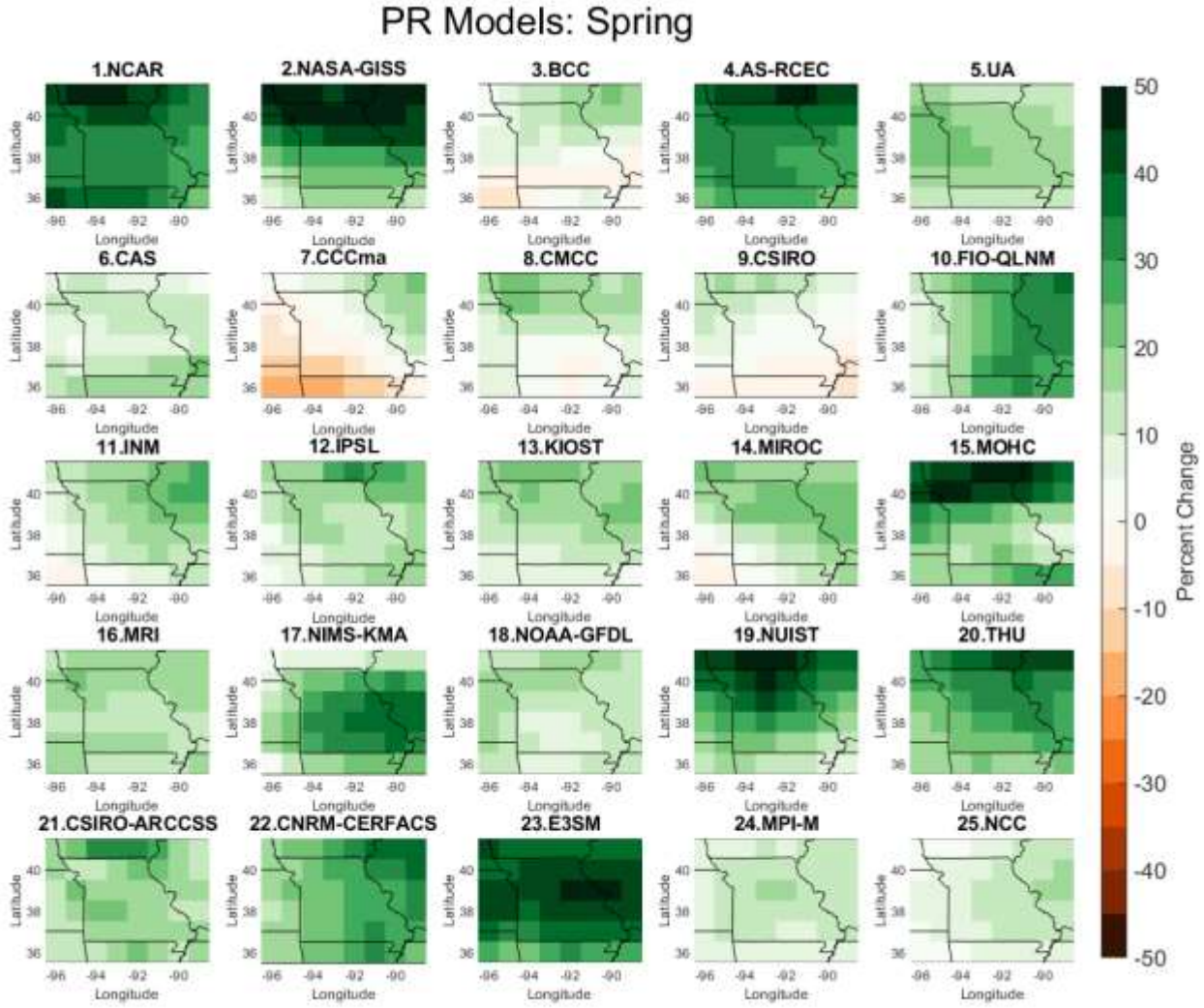

Figure 15. Mean spring precipitation precent change between SSP5-8.5 and Historical for each model.

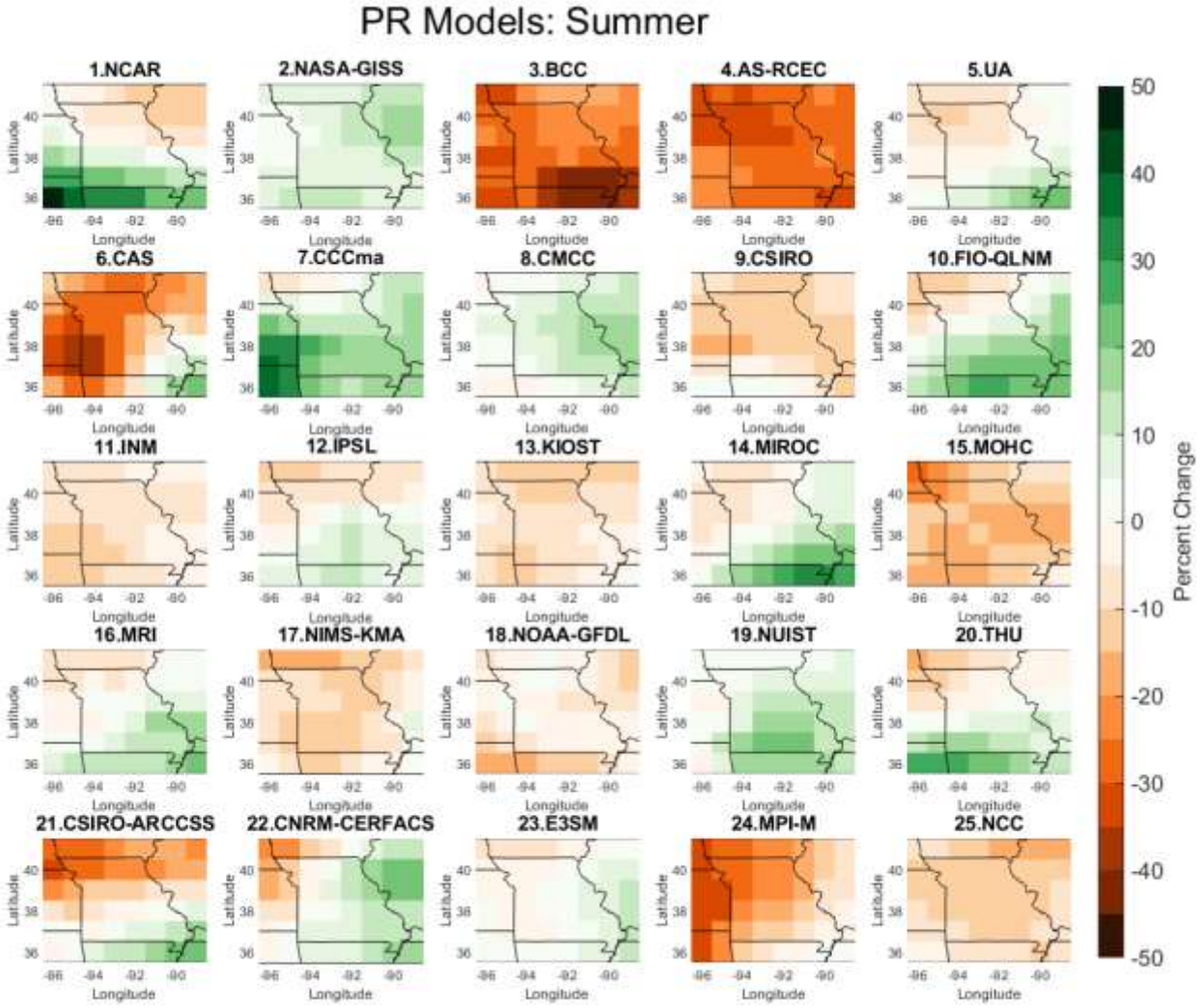

Figure 16. Mean summer precipitation precent change between SSP5-8.5 and Historical for each model.

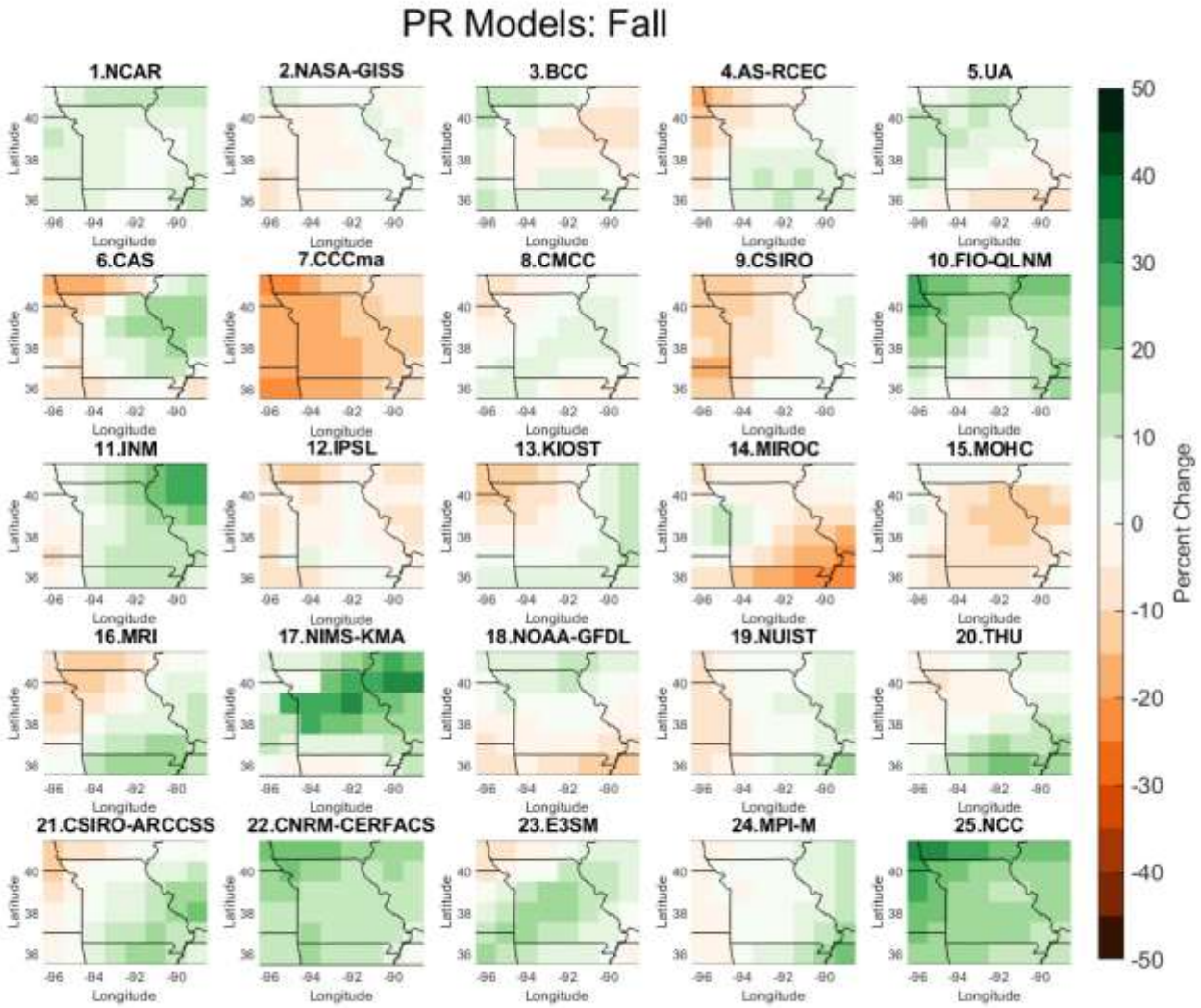

Figure 17. Mean fall precipitation precent change between SSP5-8.5 and Historical for each model.

3.2.2 Area Mean Evaluation

Area means were calculated for the annual and seasonal precipitation percent change results by averaging the precipitation percent change values from each model's grid cells. The maps were suitable for identifying spatial trends. However, the area mean can transform the data into a single value representing each model, which is helpful for comparison and analysis. Figures 18 and 19 illustrate the area annual mean and seasonal mean as bar charts. The annual bar chart had all models with a positive percent change, suggesting an unanimously wetter projection for the area. The seasonal bar chart had a diverse range of results. The winter and spring season results all had a positive percent change. The summer season results had a mix of positive (wetter) and negative (drier) percent changes, while the fall season had a small number of negative percent changes. The mean, median, standard deviation, maximum, minimum, and range were calculated for the area mean and can be found in Table 4. Notable results from statistics were that winter had the largest maximum, spring had the largest mean, and summer had the largest range.

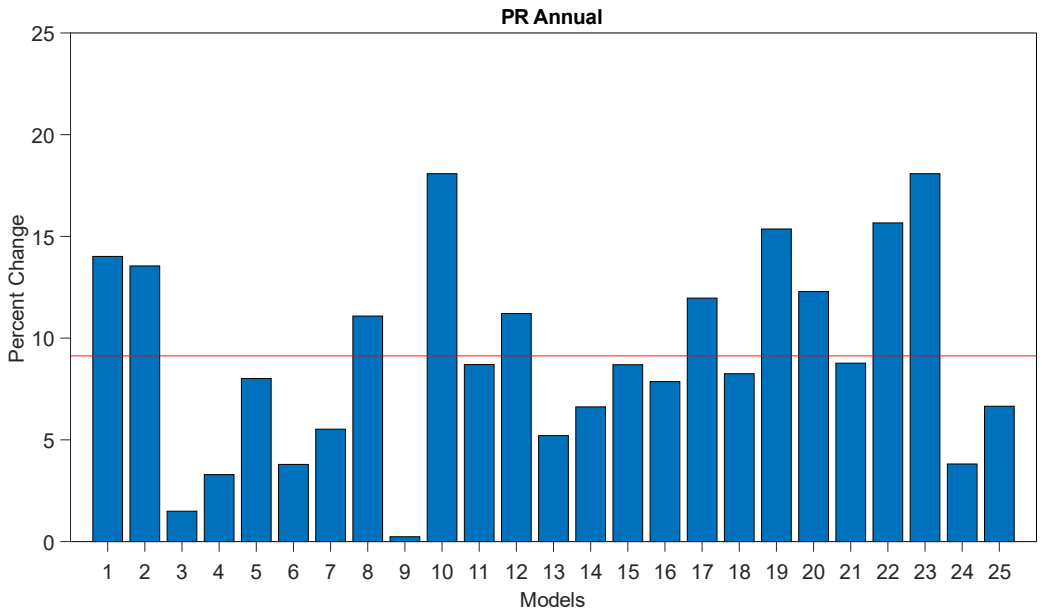

Figure 18. Area annual mean precipitation percent change of each model. The red line is the ensemble mean of all the models.

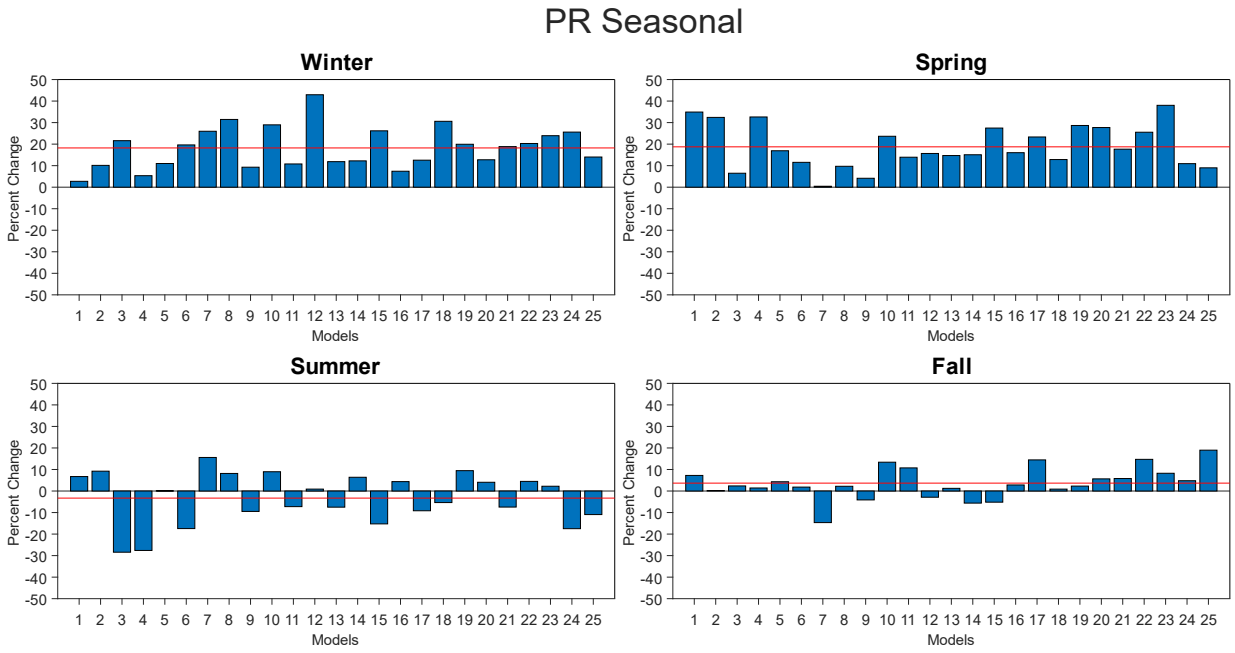

Figure 19. Area seasonal mean precipitation percent change of each model. The red line is the mean of all the models.

Table 4. Descriptive statistics from the area mean precipitation percent change of all models.

	Winter	Spring	Summer	Fall	Annual
Mean	18.24	18.77	-3.31	3.64	9.13
Median	18.84	16.03	0.09	2.36	8.69
Standard Deviation	9.61	10.12	11.79	7.38	4.94
Maximum	42.93	38.02	15.59	18.98	18.08
Minimum	2.73	0.44	-28.42	-14.67	0.24
Range	40.20	37.58	44.01	33.65	17.84

3.3 Heatmap Summary

Two heat maps were created to help summarize the wind speed and precipitation change results. Heat maps are a good summary tool because they condense much information into one organized figure. The heat maps in this study have the seasons listed as columns and the models listed as rows. The heat maps can be used to compare model results for individual seasons or to see the trend of each model across the seasons.

Figure 20 presents the wind speed heat map. The heat map shows most models having a decrease in wind speed across all seasons ranging from -0.03 to -0.69 meters per second. The winter, spring, and fall have a mix of increasing and decreasing wind speeds, while in the fall, all models showed a decrease in wind speed. Model 8 stood out in the heat map because it had wind speed increasing consistently across most seasons and had the largest increase during spring at 0.25 meters per second. Model 11 also stood out in the heat map because it had a massive wind speed decrease across most seasons and had the greatest decrease during fall at -0.69 meters per second.

The precipitation percent change heat map is detailed in Figure 21. Most models in the heat map have a 0 to 10 percent change. The winter and spring seasons have a larger positive percent change, while the summer and spring have a mix of positive and negative percent

change. The most considerable positive percent change was model 12, with ~43% wetter during the winter, and the most prominent negative percent change was model 3, with ~-28% dryier in summer. Most models during the summer season had a negative percent change. However, all models had a positive percent change annually speaking. The model that stood out in the heat map was model 4, which had a nearly 33 percent increase in precipitation during the spring and a -28 percent decrease for the summer, which is a massive shift.

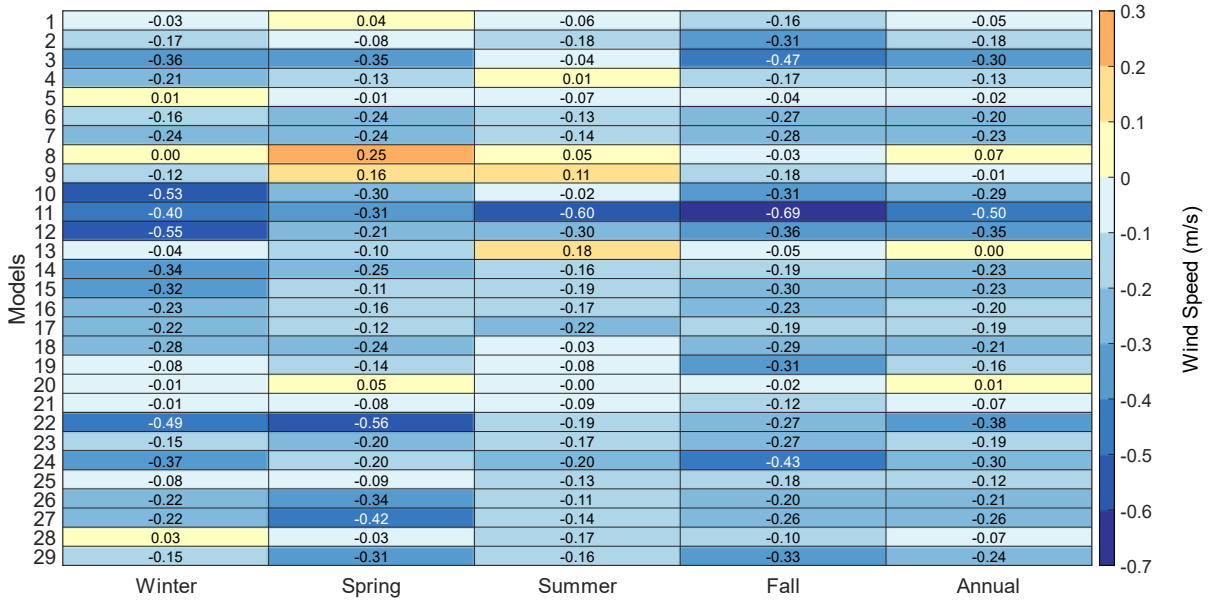

Figure 20. Heatmap of area means of wind speed difference for each model.

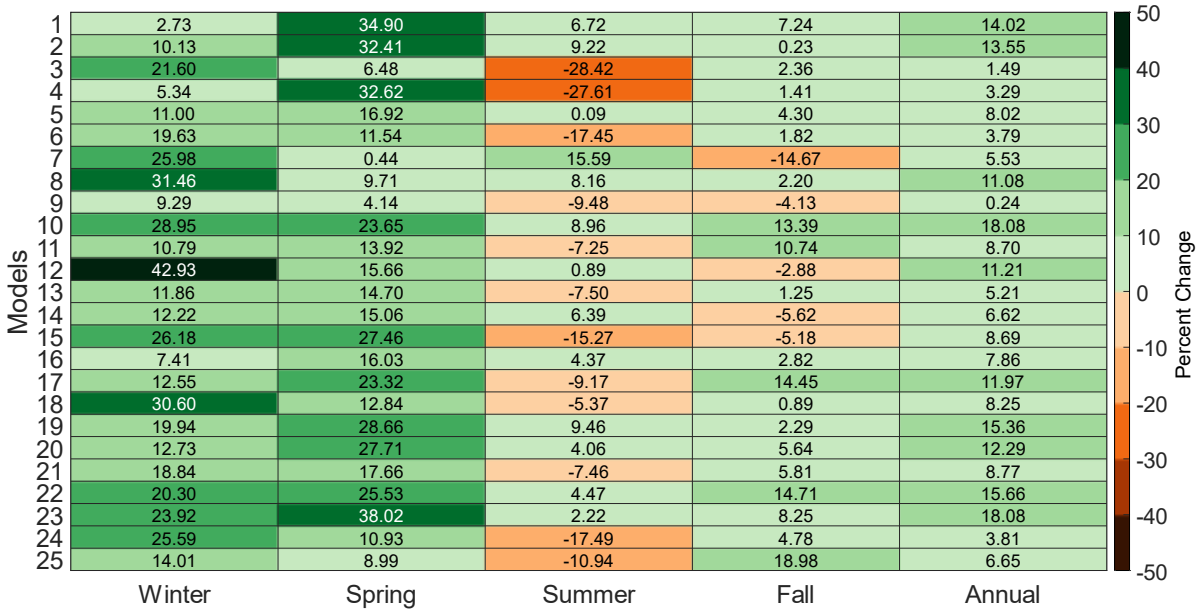

Figure 21. Heatmap of area means of precipitation percent change for each model.

CHAPTER 4

RESULTS: EXTREME CHANGE

4.1 Winter Wind Speed Extremes

The threshold used to assess winter wind speed extremes was a 95th percentile threshold. A unique threshold was calculated using the 95th percentile of the Historical daily wind speed data. The unique threshold was then utilized to find the number of extreme wind speed days per year for the SSP5-8.5 future scenario. Then, the difference between the SSP5-8.5 future scenario and Historical was calculated to examine the change in the number of days per year. Figure 22 first illustrates the calculated unique threshold wind speeds for each model and each grid cell. All models had a 95th percentile threshold wind speed greater than or equal to 3.5 meters per second. Most models had a threshold range of 3.5 to 11 meters per second. The threshold values spatially varied for many models. The greatest threshold wind speed was generally in the northern areas and was very apparent for models 11, 12, 25, 26, and 27. The 95th percentile days per year difference results varied across all the models in Figure 23. The days per year results ranged from -4 to 2. Models 11, 12, 22, and 24 displayed larger negative days per year, while models 1, 19, 20, 21, and 28 displayed positive days per year results. There are mixed results for the winter wind speed extremes, with some models presenting more extreme windy days while others show less extreme windy days in the future. Figure 24 shows the ensemble-mean 95th percentile days per year difference for all the models from Figure 23. It was negative across the entire study area and had the largest negative value in the southwest of Missouri.

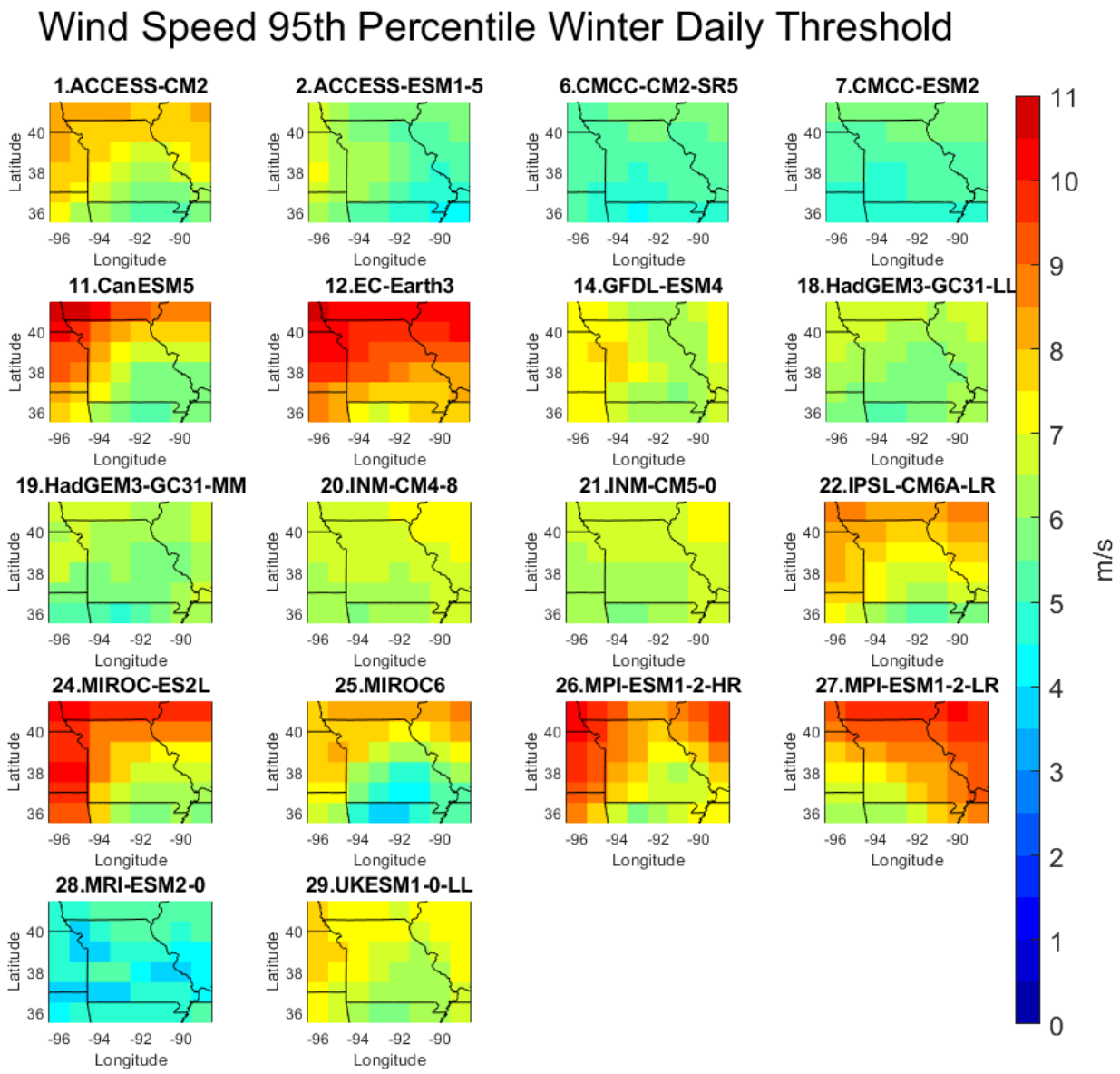

Figure 22. Historical 95th percentile winter wind speed for each model grid cell.

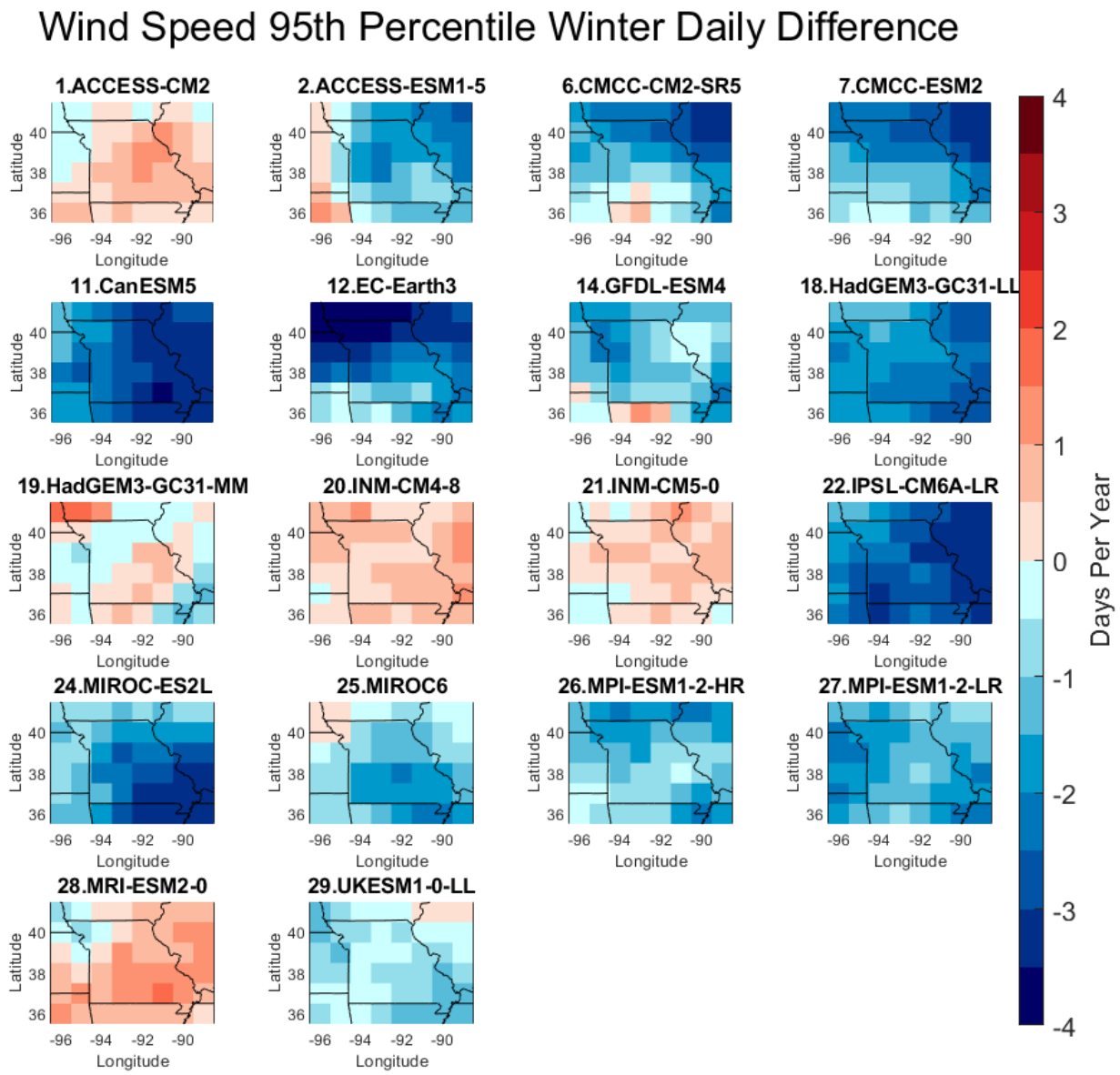

Figure 23. The number of days per year difference between SSP5-8.5 and Historical winter wind speed by using the 95th percentile Historical wind speeds as a threshold for each model grid cell.

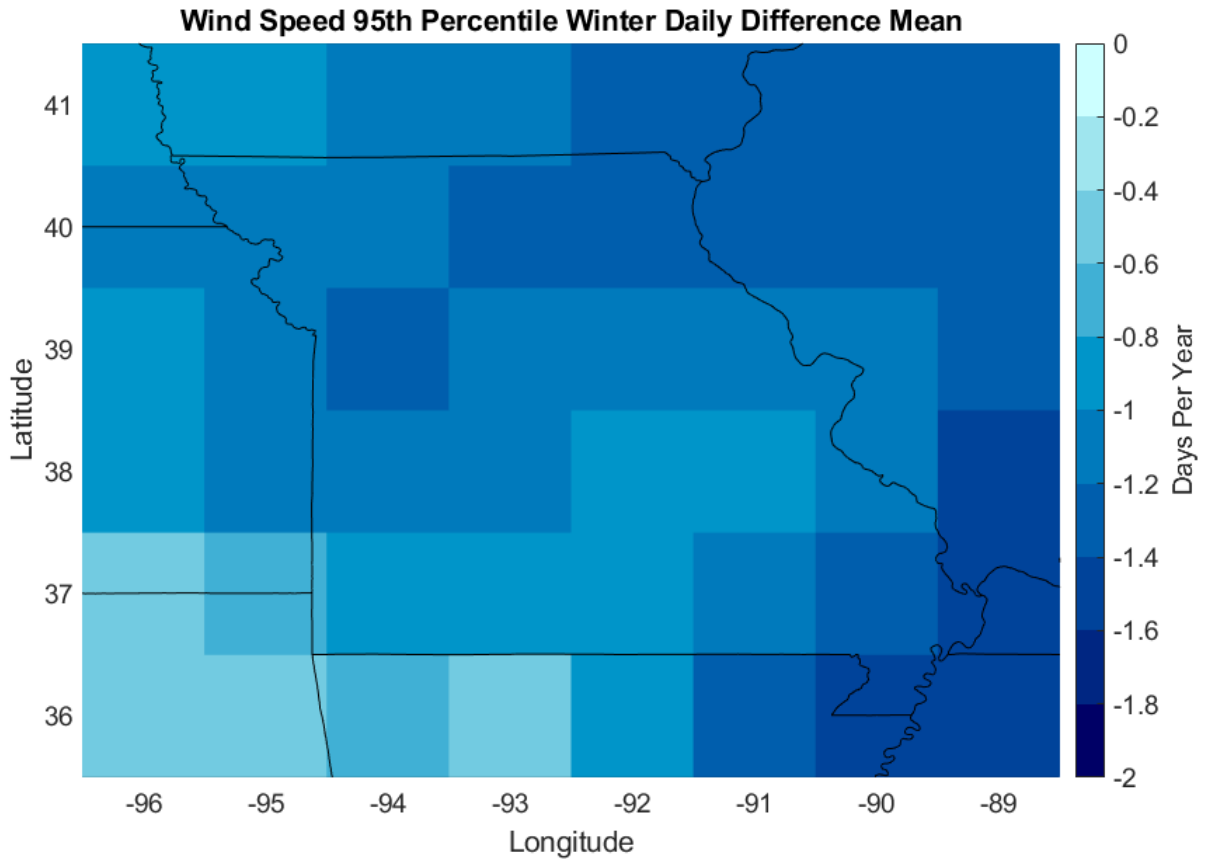

Figure 24. The ensemble-mean number of days per year difference between SSP5-8.5 and Historical winter wind speed when using the 95th percentile Historical wind speeds as a threshold.

4.2 Summer Wind speed Extremes

Similarly, a 95th Percentile Threshold was used to examine summer wind speed extremes. First, the Historical daily wind speed data's 95th percentile values were used as the unique threshold values. Next, the change of the number of days per year between SSP5-8.5 and Historical was calculated using the unique threshold. Then, the change in the number of days per year was calculated by subtracting the SSP5-8.5 and Historical results. The unique 95th percentile thresholds of wind speed are first plotted in Figure 25. It ranged between 1.5 and 9.5 meters per second. Models 25 and 28 had very low wind speed thresholds compared to the other models. A general pattern among the models was that the western areas had a higher wind speed threshold than the others. Figure 26 shows the change in the number of days per year between SSP5-8.5 and Historical. As it shows that the change in the number of extremely windy summer days varies substantially. There tended to be fewer extremely windy days in the northern areas while more in the southern areas. The range of days per year change was around -4 to 3. The models that stood out were 7 and 12 because they both had areas with larger negative and positive days per year results. The average across all the models is detailed in Figure 27. The ensemble-mean change shows a decrease in the extremely windy days for the entire study area and it is evident that the most significant decrease was in the north of the region while a slight decrease seen in the south.

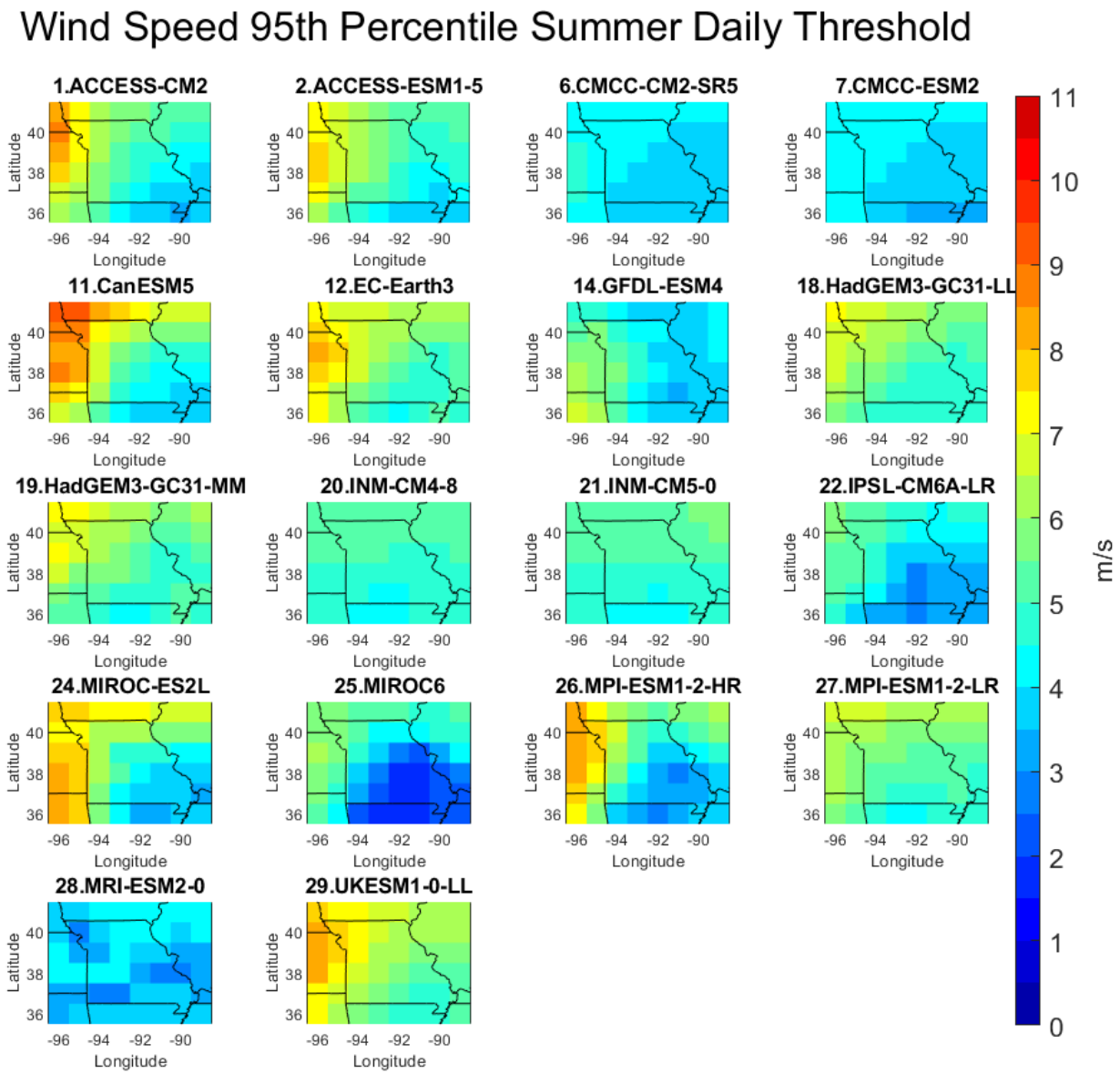

Figure 25. Historical 95th percentile summer wind speed for each model grid cell.

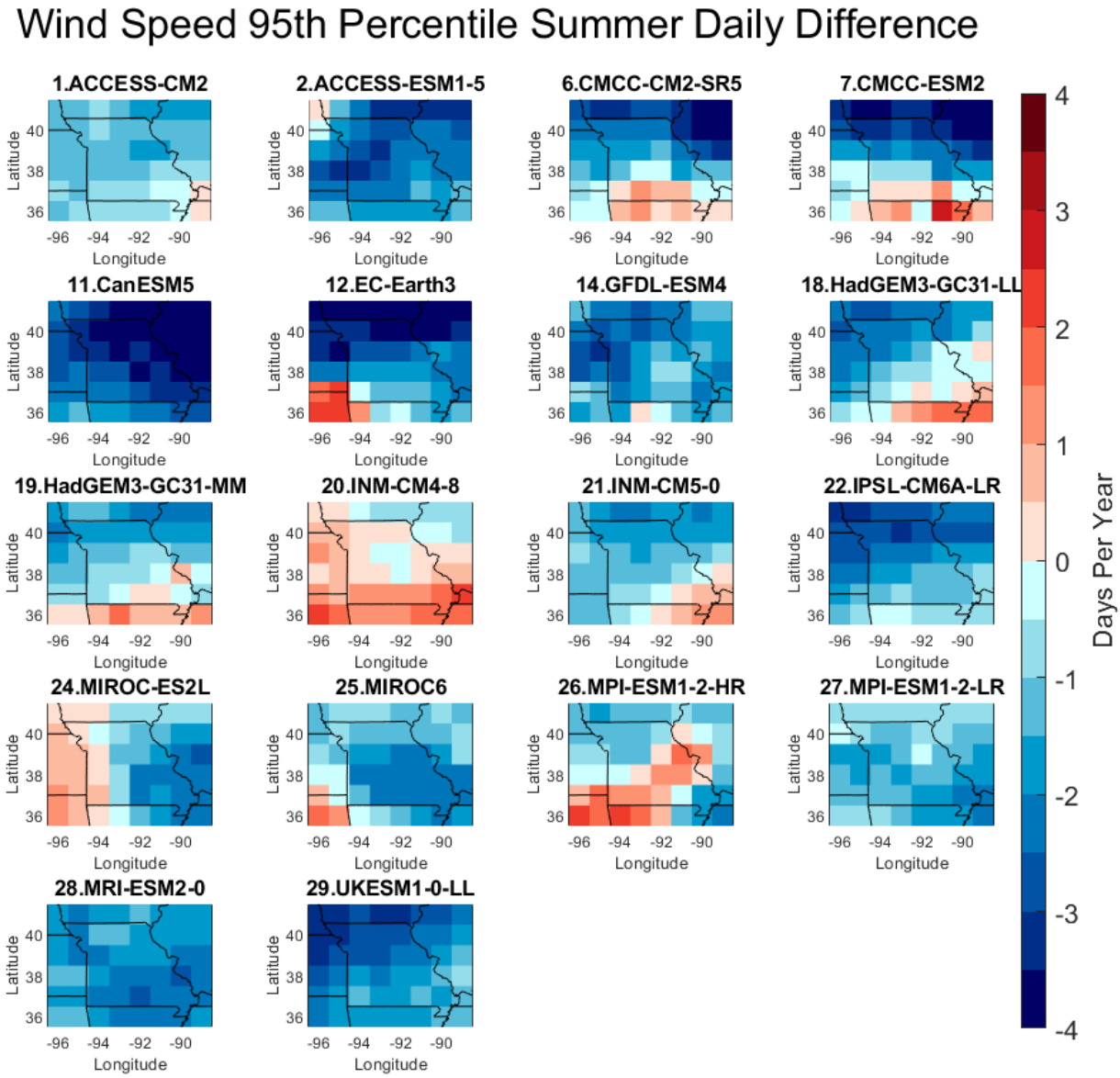

Figure 26. The number of days per year difference between SSP5-8.5 and Historical summer wind speeds by using the 95th percentile Historical wind speeds as a threshold for each model grid cell.

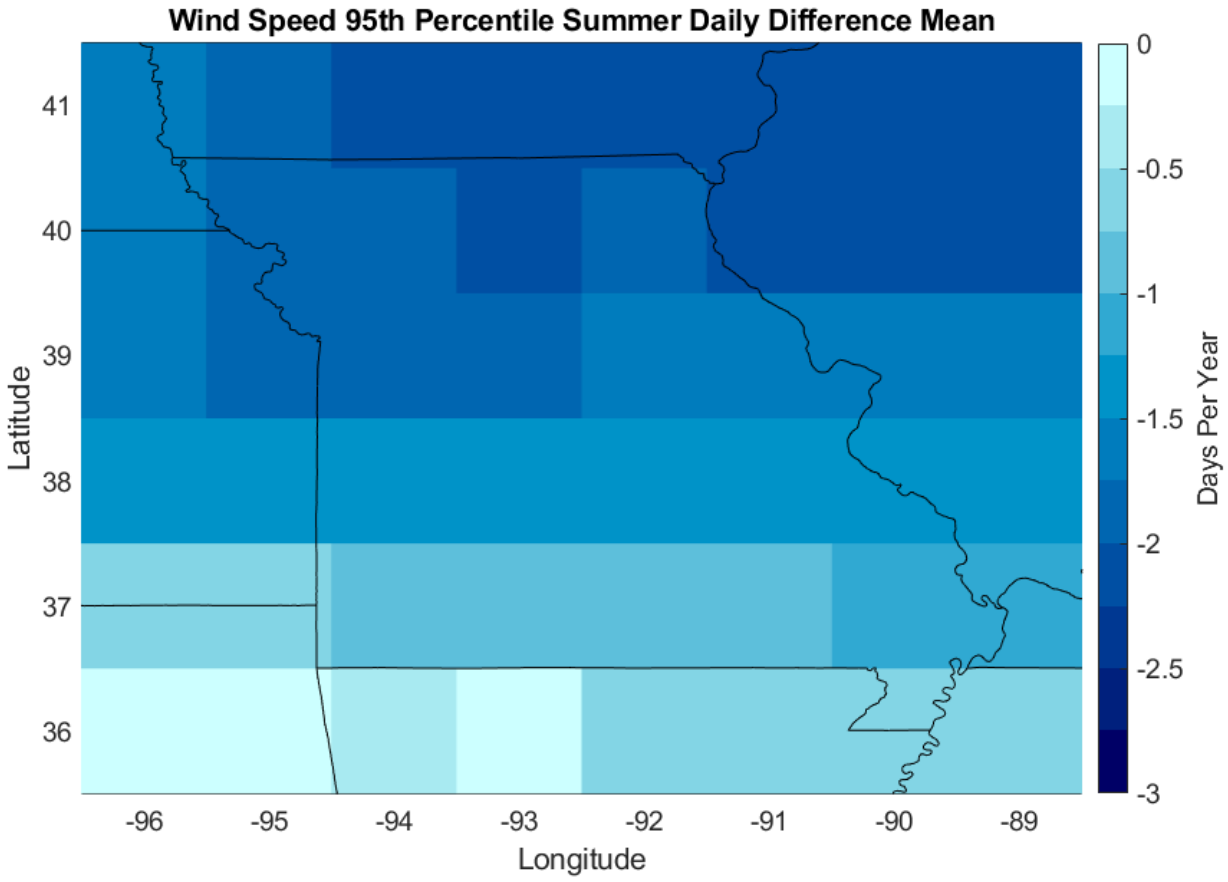

Figure 27. The ensemble-mean number of days per year difference between SSP5-8.5 and Historical summer wind speeds when using the 95th percentile Historical wind speeds as a threshold.

4.3 Winter Precipitation Extremes

The threshold used to assess winter precipitation extreme was a 95^{th} percentile threshold. The Historical daily precipitation data's 95^{th} percentile values were quantified as the unique threshold values. The SSP5-8.5 precipitation days per year change was calculated using this unique threshold. Then, the change in the number of extreme precipitation days was calculated by subtracting the SSP5-8.5 and Historical results. The spatial patterns of threshold values for each model are shown in Figure 28, ranging from 5 to 25 mm per day. They are similar across all models, with the smallest values in the northwest and the largest values in the southeast of the region. The changes of the number of extreme precipitation days between SSP5-8.5 and Historical is presented in Figure 29. All the models have very different spatial patterns. It shows that most models have a general increase of extreme days across the whole region, except models 1, 3, 4, and 16, with a sizable decrease in certain areas. The largest increase was about four days per year, almost doubling the number of extreme precipitation days in Historical, while the largest decrease was around -1.5 days per year. Figure 30 shows the ensemble mean of the change, with an increase across the whole region.

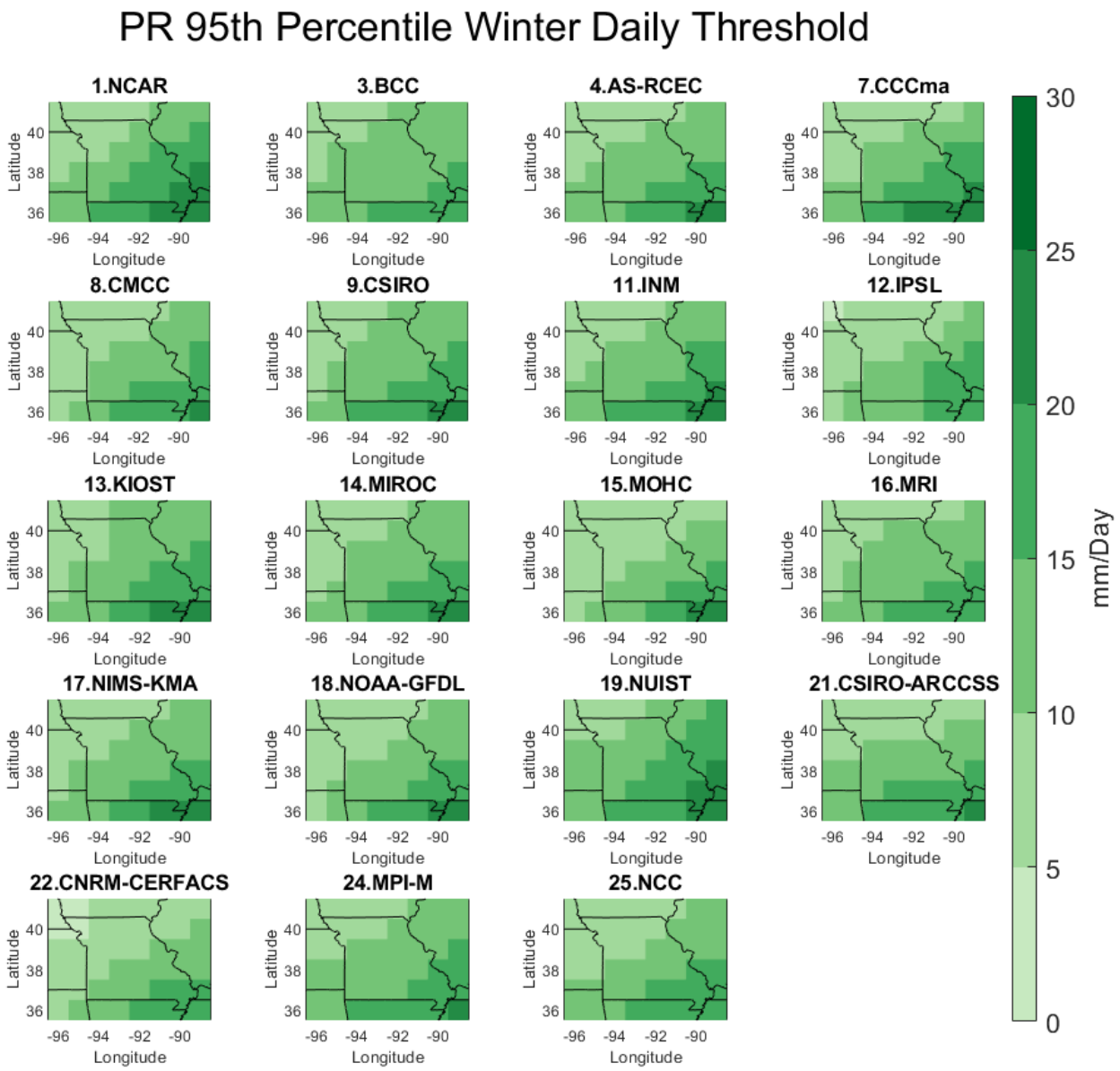

Figure 28. Historical 95th percentile winter precipitation for each model grid cell.

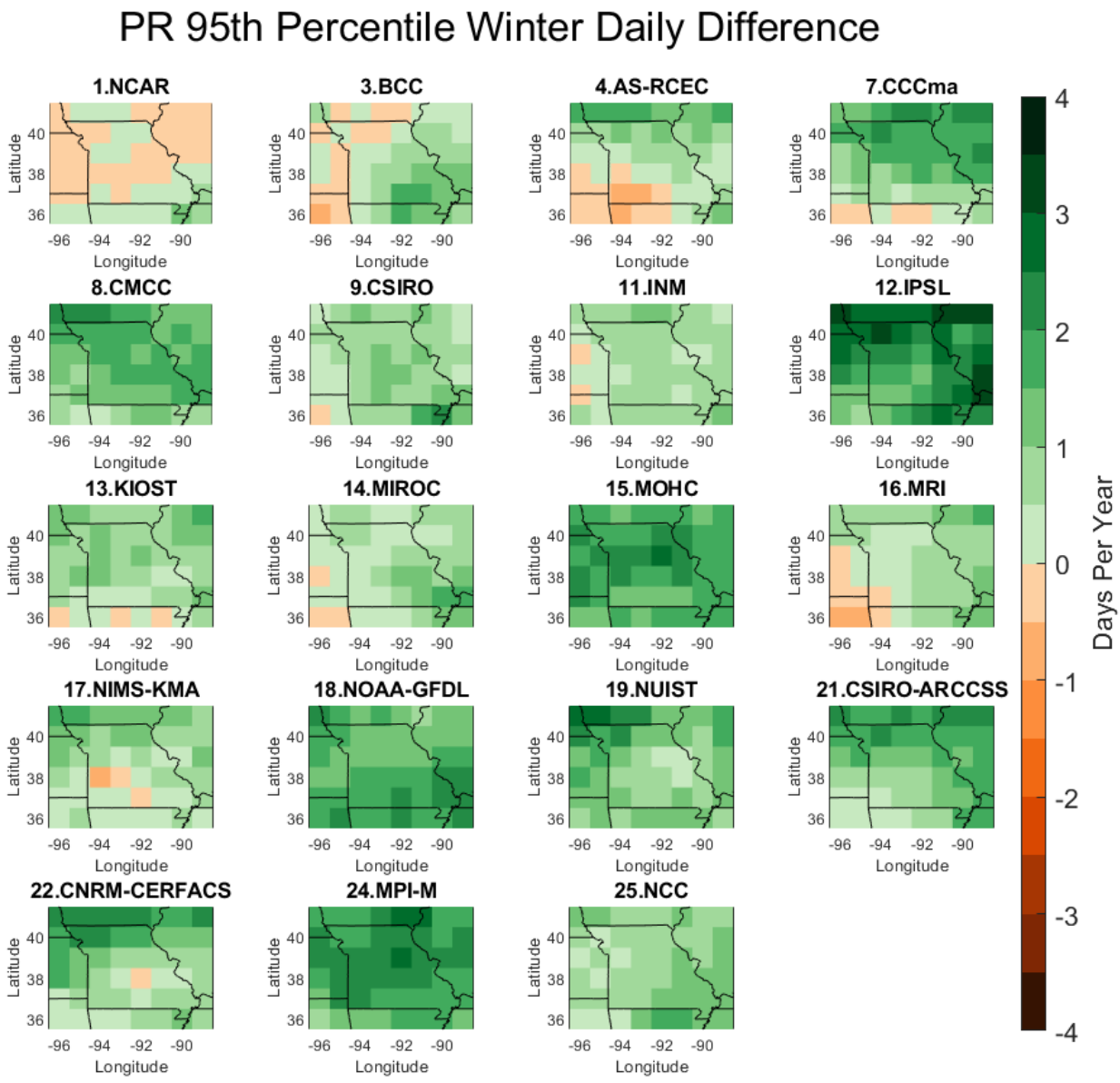

Figure 29. The number of days per year difference between SSP5-8.5 and Historical winter precipitation by using the 95th percentile Historical winter precipitation as a threshold for each model grid cell.

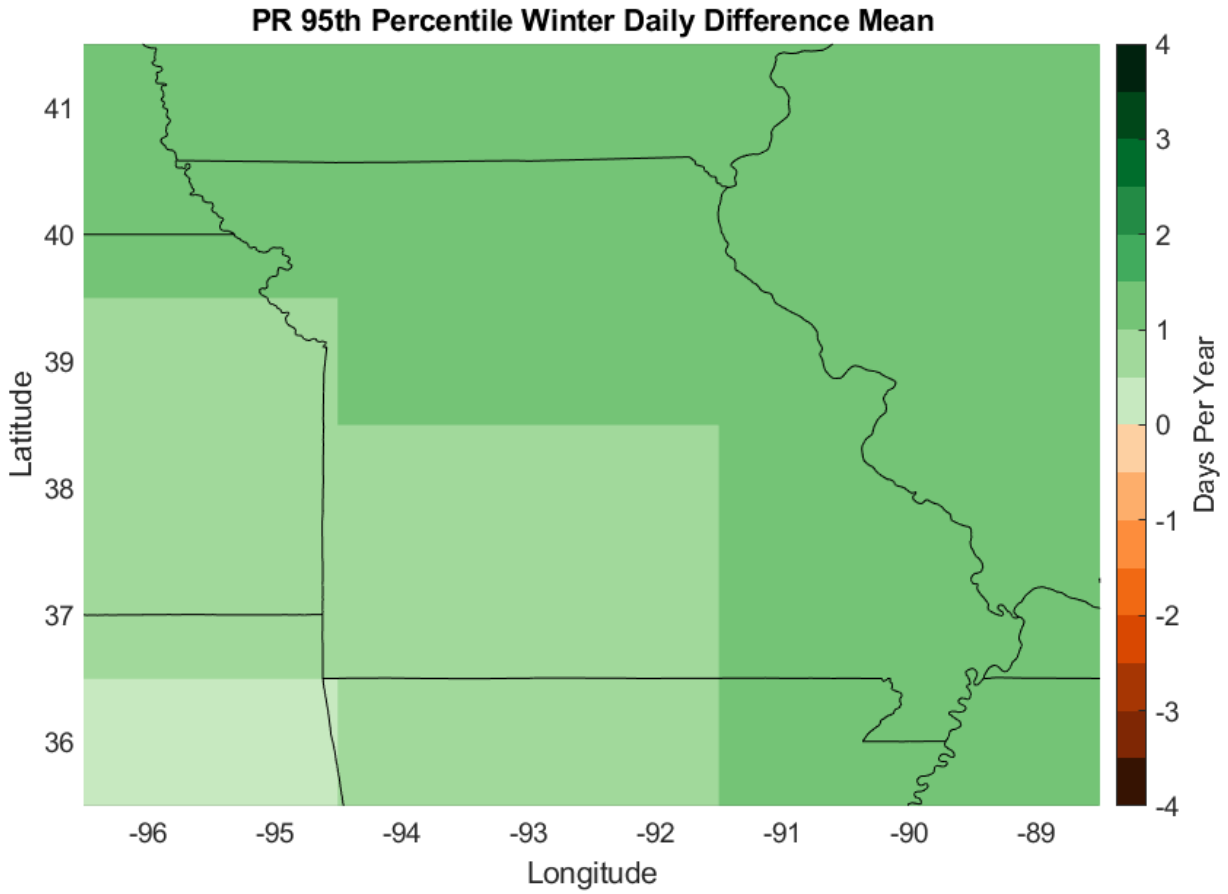

Figure 30. The ensemble-mean of the number of days per year difference between Historical and SSP5-8.5 winter precipitation when using the 95th percentile Historical winter precipitation as a threshold.

4.4 Summer Precipitation Extremes

A 95th percentile threshold was used to examine summer precipitation extremes. First, a unique threshold was calculated using the 95th percentile of the Historical summer daily precipitation data. The unique threshold was then utilized to find the number of summer extreme precipitation days for the SSP5-8.5. Then, the difference between SSP5-8.5 and Historical was calculated to examine the changes. The thresholds calculated from the summer Historical data can be found in Figure 31. The threshold values varied from 2.5 to 25 mm per day. A varying spatial pattern is observed across all the models. Figure 32 illustrates the change in the number of summer extreme precipitation days. A majority of the models show generally reduced number of extreme days, while a few shows a mixture of increase and reduction. The change of number of days ranged from -4 to 4 days per year. Models 3, 4, 13, and 15 stood out in the figure with the entire study area all negative values. The ensemble-mean difference for the summer precipitation extremes is further explored in Figure 33. It shows mostly negative values except the southeast corner of the region, indicating the generally reduced number of extreme precipitation in summer.

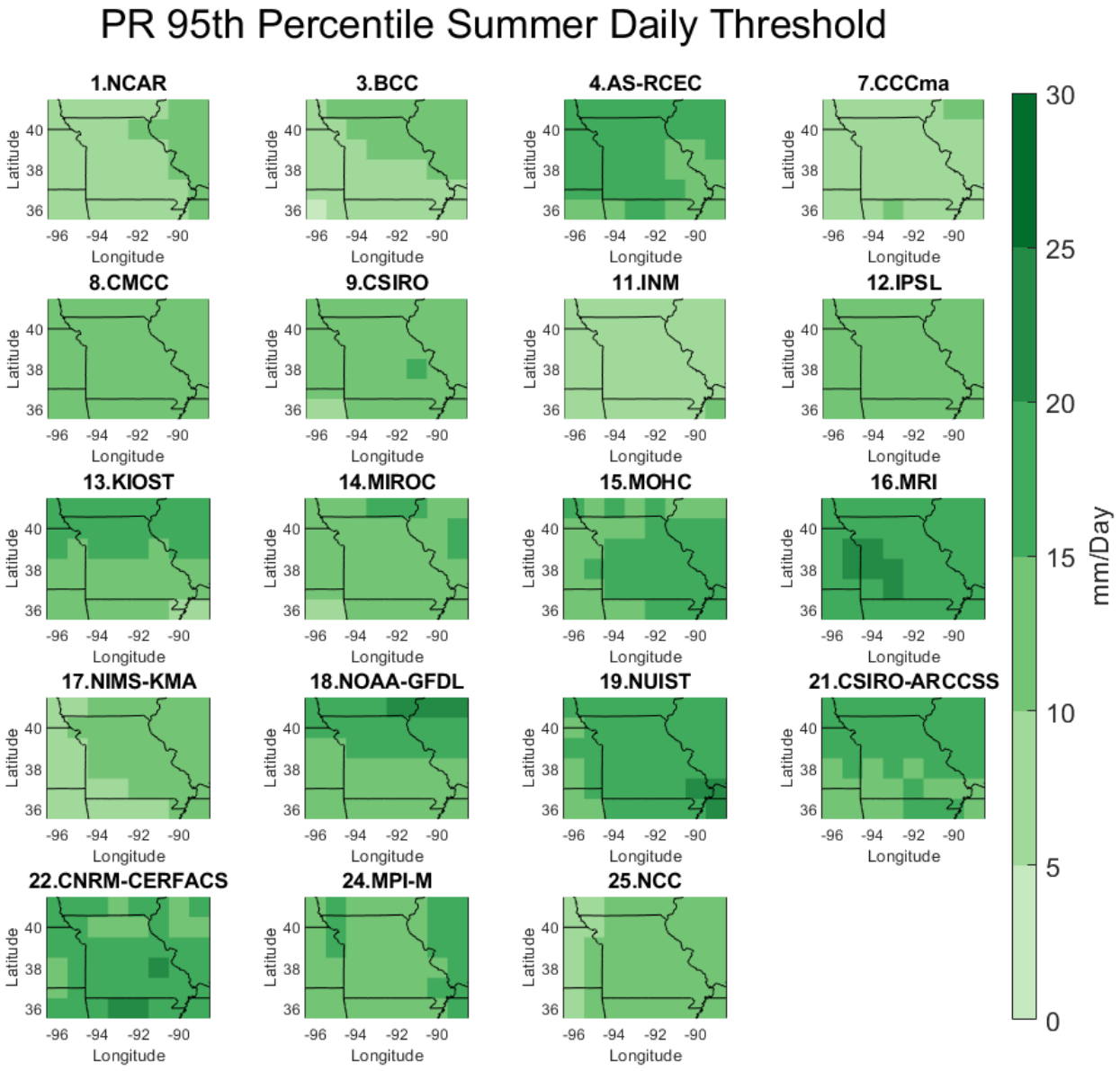

Figure 31. Historical 95th percentile summer precipitation for each model grid cell.

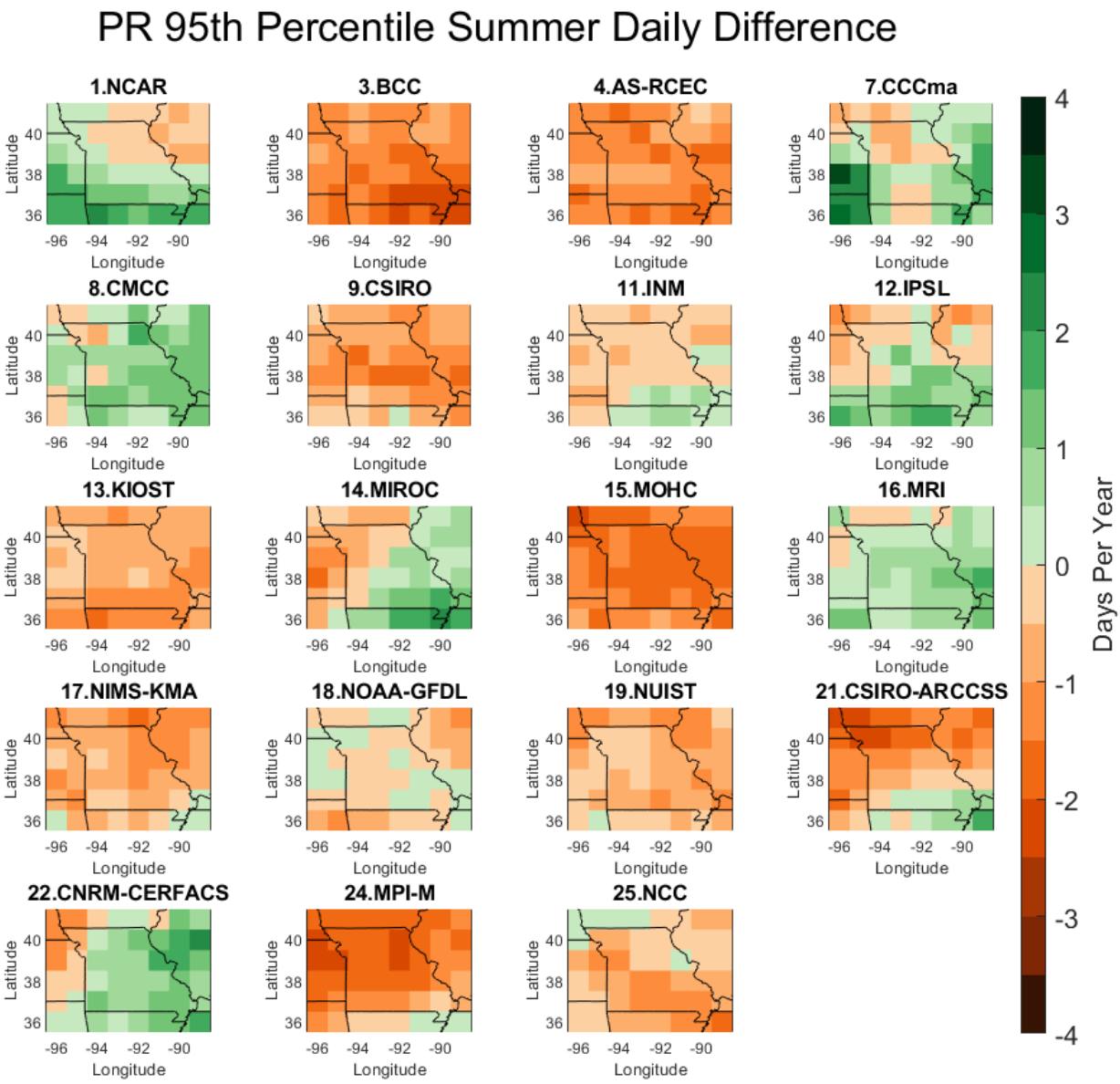

Figure 32. The number of days per year difference between SSP5-8.5 and Historical summer precipitation by using the 95th percentile Historical summer precipitation as a threshold for each model grid cell.

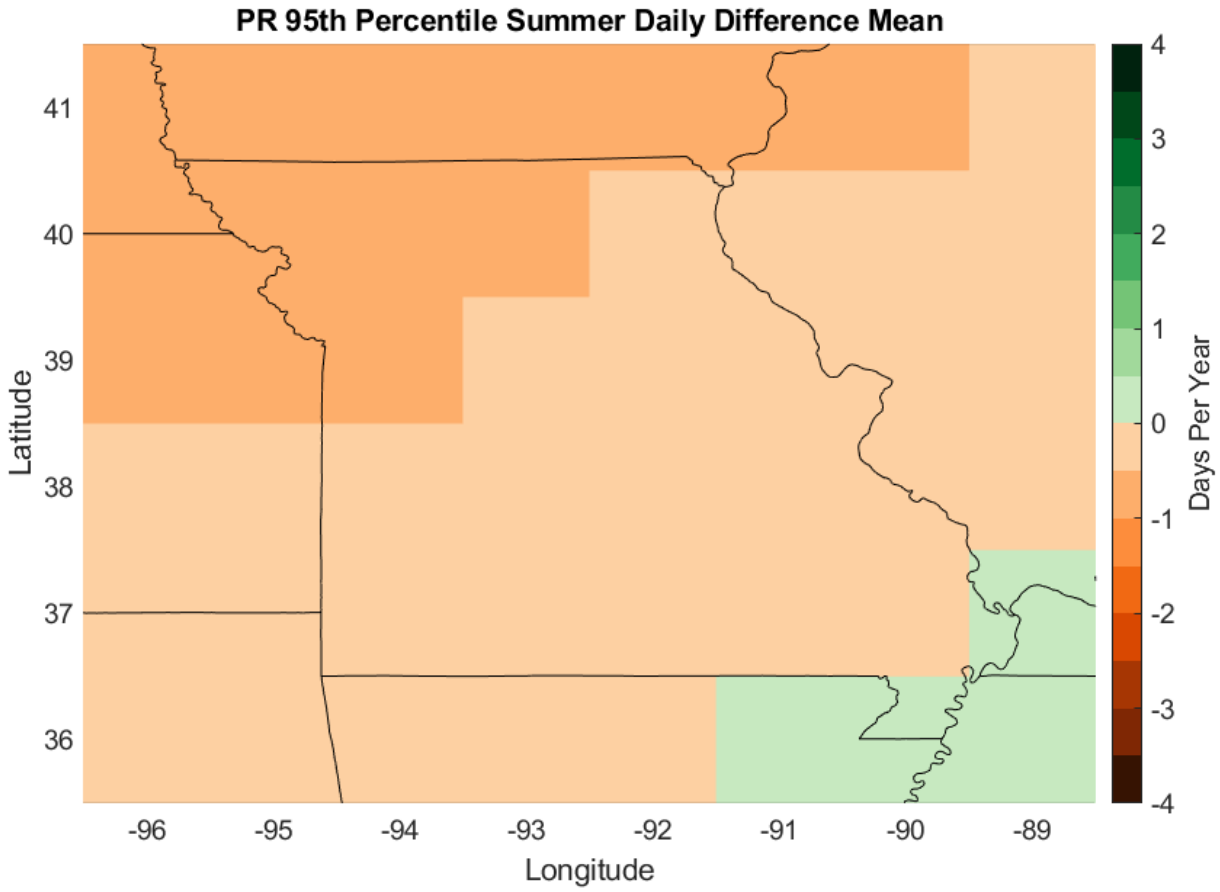

Figure 33. The ensemble-mean of the number of days per year difference between Historical and SSP5-8.5 summer precipitation when using the 95th percentile Historical summer precipitation as a threshold.

CHAPTER 5

DISCUSSION AND CONCLUSION

5.1 Annual and Seasonal Wind Speed Change and Its Impacts on Broadband Infrastructure

With the analysis of the CMIP6 global climate model simulations, we found a general decrease in the annual-mean wind speed in Missouri by the end of the 21st century in the business-as-usual greenhouse gas emissions scenario compared to the baseline. Most climate models show the most significant wind speed decrease in the northern areas of Missouri. The models that show increases in wind speed tend to be in the south and southwest of the state. The model-to-model disagreements indicate there are some uncertainties across the models' projections in the future. Analysis of the state average shows that wind speed decreases across almost all models with an ensemble-mean decrease of 0.18 meters per second with a standard deviation of 0.13 meters per second (Table 3).

Further analysis of the seasonal-mean wind speed change presents a more significant wind speed decrease, especially in the northern parts of Missouri in the winter and fall seasons. During the winter and fall seasons, nearly all of the models show a decrease in wind speed, while the spring and summer show a mix of models with an increased or decreased wind speed. In the spring and summer seasons, some models show an increase in wind speed, particularly to the southwest of the region. The results show a seasonal dependence of the changes in the surface wind speed. The area means' statistics in Table 3 and the bar charts in Figure 10 continued to support that the winter and spring seasons have the greatest mean and median wind speed decrease. On the other hand, the spring and summer season's area mean had the greatest wind speed increase maximums and range. The seasonal area means described Missouri as having a greater wind speed decrease during the winter and fall seasons, while the spring and summer

seasons are expected to have greater potential for wind speed increases. These results are also consistent with the heatmap in Figure 20. The annual and seasonal maps and area mean analysis provided reasonable evidence that wind speeds will decrease across Missouri during most seasons and not be exceptionally threatening to broadband infrastructure. However, there are still some uncertainties due to the model disagreements.

5.2 Annual and Seasonal Precipitation Percent Change and Its Impacts on Broadband Infrastructure

Analysis of the annual precipitation percentage change shows an increase across the region, suggesting a wetter Missouri in the future. The largest ensemble-mean percentage increase is seen in the eastern areas of Missouri. This is partially due to the fact that some models simulate a precipitation decrease in the western areas of Missouri, which cancels off the simulated increase in precipitation by other models. However, the negative percent change observed in certain areas was minor, and the overall consensus of models shows an increase in precipitation, with the ensemble-mean area-mean percentage increase being more than 9% (Figure 18 and Table 4). It's noteworthy that the annual area mean from our study is consistent with the IPPC's projected precipitation increase over land (Lee et al. 2021).

The seasonal precipitation percent change analysis further found a substantial increase in precipitation, especially in the northern parts of Missouri during the winter and spring, a noticeable decrease during the summer, and a slight increase during the fall. The winter, spring, and summer mean percent change maps also had more of a south-to-north spatial pattern that differed from the annual percent change. Individual models for each season had a wide variety of spatial patterns (Figure 14-17) and area-mean percent change values (Figures 19 and 21). All the models' area means were in agreement during the winter and spring seasons that precipitation

would increase with an ensemble-mean value of more than 18% for both seasons, while the summer season had many models that substantially disagreed on whether precipitation would increase or decrease, yielding to an ensemble-mean value of over 3% decrease. The fall season results had most models agreeing that a slight precipitation increase (nearly 4%) would occur. The precipitation percent change varies significantly, depending on seasons. The annual, winter, and spring see large increases in precipitation, corresponding to a wetter future in Missouri, while the summer shows a potentially drier future. **The substantial increase (over 18%) in total precipitation and potential surface flooding during the winter and spring may threaten broadband infrastructure.**

5.3 Winter and Summer Wind Speed Extremes

Investigation of the frequency of wintertime extremely windy days first revolved around a threshold to define an extreme. An objective 95th percentile wind speed threshold in winter season was chosen and applied to the daily surface wind speed data to quantify the changes in the number of extreme windy days between the SSP5-8.5 and Historical data. The winter wind speed thresholds displayed large spatial inhomogeneity and huge model-to-model discrepancy, which was further shown in the change of extreme windy days. More than two thirds of the models predict a decrease in the number of strong windy days while the rest nearly one third of the models predict an increase throughout Missouri. The ensemble-mean yielded to a general decrease in the number of strong windy days and the greatest decrease was seen in the southeast part of Missouri. Winter extremely windy days are predicted to potentially decrease, thus are not a major risk to broadband infrastructure though some models do show an increase across the whole state.

A similar analysis was applied to the examination of the frequency of summertime extremely windy days. A 95th percentile threshold was first calculated for summer months and then used to identify the change in the number of extremely windy days between the Historical and SSP5-8.5 data during the summer. The calculated summer threshold values were generally lower but had a slightly larger cross-model range than the winter ones. Model-to-model disagreements in the extreme changes revealed similarly mixed results to the winter season. However, the summer season showed a greater cross-model range of the change, mainly because some models predict a larger increase in the number of extremely windy days. For those models showing an increase, there is also a common spatial pattern with increases in the south and decreases in the north of Missouri. This pattern likely explains the meridional contrast in the ensemble-mean change, with greater decreases in the north compared to the south.

In conclusion, most models showed winter and summer extremely windy days decreasing across the whole of Missouri. It suggests that extremely windy speed events might not be a major threat to broadband infrastructure. However, our results found that there are models showing a substantial increase in extremely windy days in parts of Missouri, suggesting extremely windy days likely happen more frequently in these areas in the future. We found summer season has a greater potential for increased extremely windy days than the winter season, leading to potentially larger negative impacts on broadband infrastructure.

5.4 Winter and Summer Precipitation Extremes

Winter and summer daily precipitation extremes were explored using the objective 95th percentile threshold, which roughly corresponds to the daily precipitation of the wettest 5 days of each season. First, the precipitation threshold values were calculated from the Historical data's distribution for each season. Then the thresholds were used to identify the difference in the

number of days per year between the SSP5-8.5 scenario and Historical data for each season individually. The calculated winter precipitation 95th percentile threshold presented a consistent spatial pattern across all the models, largest values seen in the southeast regions of Missouri. The extreme changes from the Historical to the SSP5-8.5 scenario displayed a nearly unanimous increase almost everywhere and in nearly all models, with the number of extreme precipitation days nearly doubled in some models. The ensemble-mean change showed that the increase could be as large as 2 more days per season, equivalent to a nearly 50% increase compared to the baseline.

The calculated summer 95th percentile threshold values showed a large spatial inhomogeneity across all the models, suggesting a larger model-to-model uncertainty in simulated summer precipitation amounts. The changes to the extreme days from the Historical to the SSP5-8.5 scenario show that most models predict decreased days of extreme precipitation while only a few models predict more extreme days. This leads to decreased numbers of extreme precipitation days nearly everywhere in Missouri except for the southeast tip.

In conclusion, the results from the extreme precipitation analysis found that Missouri is expected to experience an increase in extreme precipitation events during the winter season while a decrease in extreme precipitation events during the summer season. The results also show a greater model agreement for winter than summer. **During the winter seasons, the increase in the number of extreme precipitation events could likely increase the vulnerability of the broadband infrastructure, which is likely more resilient in the summer seasons.**

5.5 Conclusions

Climate change and its adverse impacts are growing threats to Missouri and its civil infrastructure. Researchers have developed climate models to help predict future climate to help prepare and plan for future impacts. This study investigated nowadays available global climate models to examine the four potential climate change signals for the Missouri region during the end of the century in a business-as-usual greenhouse gas emissions scenario. The four climate change signals were climatological wind speed and precipitation change and the frequency change of extremely windy days and extreme precipitation events. The AOGCMs provided Historical and SSP5-8.5 scenario data that was analyzed to evaluate the four signals. The results from the mean change analysis found a decrease in wind speed annually and across all seasons, while precipitation increases annually and for all seasons except for the summer for most models analyzed. In addition, extremely windy events likely generally decreased in winter and summer, while extreme precipitation events increased during the winter and decreased in the summer. **The results indicate that Missouri's broadband infrastructure is at a greater risk of precipitation change, extreme precipitation events, and potential surface flooding compared to the changes in the surface wind speed.**

A caveat of this study was the use of only one future greenhouse gas emissions scenario, while the IPCC AR6 proposed a handful of core various scenarios. The future scenario used in this study is considered the worst-case emissions scenario. However, the future is uncertain, and the selected scenario in this study might not reflect future conditions best. CMIP6 provides many different scenarios that could be explored in future research to examine the wider range and larger uncertainty of mean climate change and extreme change. Further research could also focus on developing a regional climate downscaling framework to study the regional climate and climate change on a finer spatial scale.

REFERENCES

Agrawala, S., 1998: Context and early origins of the Intergovernmental Panel on Climate Change. *Clim. Change*, **39**, 605–620.

Bader, D. C., R. Leung, M. Taylor, and R. B. McCoy, 2019: E3SM-Project E3SM1.1 model output prepared for CMIP6 CMIP historical https://doi.org/10.22033/ESGF/CMIP6.11485.

——, ——, ——, and ——, 2020: E3SM-Project E3SM1.1 model output prepared for CMIP6 ScenarioMIP ssp585. https://doi.org/10.22033/ESGF/CMIP6.15179.

Bolin, B., 2007: *A History of The Science and Politics of Climate Change: The Role of The Intergovernmental Panel on Climate Change*. Cambridge University Press, 277 pp.

Boucher, O., and Coauthors, 2018: IPSL IPSL-CM6A-LR model output prepared for CMIP6 CMIP historical. https://doi.org/10.22033/ESGF/CMIP6.5195.

——, and Coauthors, 2019: IPSL IPSL-CM6A-LR model output prepared for CMIP6 ScenarioMIP ssp585. https://doi.org/10.22033/ESGF/CMIP6.5271.

Byun, Y.-H., and Coauthors, 2019a: NIMS-KMA KACE1.0-G model output prepared for CMIP6 ScenarioMIP ssp585. https://doi.org/10.22033/ESGF/CMIP6.8456.

——, Y.-J. Lim, H. M. Sung, J. Kim, M. Sun, and B.-H. Kim, 2019b: NIMS-KMA KACE1.0-G model output prepared for CMIP6 CMIP historical. https://doi.org/10.22033/ESGF/CMIP6.8378.

Cao, J., 2019: NUIST NESMv3 model output prepared for CMIP6 ScenarioMIP ssp585. https://doi.org/10.22033/ESGF/CMIP6.8790.

——, and B. Wang, 2019: NUIST NESMv3 model output prepared for CMIP6 CMIP historical. https://doi.org/10.22033/ESGF/CMIP6.8769.

Chai, Z., 2018: CAS CAS-ESM1.0 model output prepared for CMIP6 ScenarioMIP ssp585.

——, 2020: CAS CAS-ESM1.0 model output prepared for CMIP6 CMIP historical.

Danabasoglu, G., 2019a: NCAR CESM2-WACCM model output prepared for CMIP6 CMIP historical. https://doi.org/10.22033/ESGF/CMIP6.10071.

——, 2019b: NCAR CESM2-WACCM model output prepared for CMIP6 ScenarioMIP ssp585. https://doi.org/10.22033/ESGF/CMIP6.10115.

Dix, M., and Coauthors, 2019a: CSIRO-ARCCSS ACCESS-CM2 model output prepared for CMIP6 CMIP historical. https://doi.org/10.22033/ESGF/CMIP6.4271.

——, and Coauthors, 2019b: CSIRO-ARCCSS ACCESS-CM2 model output prepared for CMIP6 ScenarioMIP ssp585. https://doi.org/10.22033/ESGF/CMIP6.4332.

EC-Earth Consortium (EC-Earth), 2019a: EC-Earth-Consortium EC-Earth3 model output prepared for CMIP6 CMIP historical.

——, 2019b: EC-Earth-Consortium EC-Earth3 model output prepared for CMIP6 ScenarioMIP ssp585.

Edwards, P. N., 2011: History of climate modeling. *Wiley Interdiscip. Rev.: Climate Change*, **2**, 128–139.

Eyring, V., S. Bony, G. A. Meehl, C. A. Senior, B. Stevens, R. J. Stouffer, and K. E. Taylor, 2016: Overview of the Coupled Model Intercomparison Project Phase 6 (CMIP6) experimental design and organization. *Geosci. Model Dev.*, **9**, 1937–1958.

Good, P., 2020: MOHC HadGEM3-GC31-LL model output prepared for CMIP6 ScenarioMIP ssp585. https://doi.org/10.22033/ESGF/CMIP6.10901.

——, A. Sellar, Y. Tang, S. Rumbold, R. Ellis, D. Kelley, and T. Kuhlbrodt, 2019: MOHC UKESM1.0-LL model output prepared for CMIP6 ScenarioMIP ssp585.

https://doi.org/10.22033/ESGF/CMIP6.6405.

Hajima, T., and Coauthors, 2019: MIROC MIROC-ES2L model output prepared for CMIP6 CMIP historical.

Harrower, M., and C. A. Brewer, 2003: ColorBrewer. org: an online tool for selecting colour schemes for maps. *Cartogr. J.*, **40**, 27–37.

Huang, W., 2019: THU CIESM model output prepared for CMIP6 CMIP historical. https://doi.org/10.22033/ESGF/CMIP6.8843.

——, 2020: THU CIESM model output prepared for CMIP6 ScenarioMIP ssp585. https://doi.org/10.22033/ESGF/CMIP6.8863.

Jackson, L., 2020: MOHC HadGEM3-GC31-MM model output prepared for CMIP6 ScenarioMIP ssp585.

John, J. G., and Coauthors, 2018: NOAA-GFDL GFDL-ESM4 model output prepared for CMIP6 ScenarioMIP ssp585. https://doi.org/10.22033/ESGF/CMIP6.8706.

Jungclaus, J., and Coauthors, 2019: MPI-M MPI-ESM1.2-HR model output prepared for CMIP6 CMIP historical.

Kim, Y., Y. Noh, D. Kim, M.-I. Lee, H. J. Lee, S. Y. Kim, and D. Kim, 2019a: KIOST KIOST-ESM model output prepared for CMIP6 CMIP historical. https://doi.org/10.22033/ESGF/CMIP6.5296.

——, ——, ——, ——, ——, ——, and ——, 2019b: KIOST KIOST-ESM model output prepared for CMIP6 ScenarioMIP ssp585. https://doi.org/10.22033/ESGF/CMIP6.11249.

Krasting, J. P., and Coauthors, 2018: NOAA-GFDL GFDL-ESM4 model output prepared for CMIP6 CMIP historical. https://doi.org/10.22033/ESGF/CMIP6.8597.

Lee, J.-Y., and Coauthors, 2021: Future global climate: scenario-based projections and near-term information. *Climate Change 2021: The Physical Science Basis. Contribution of Working Group I to the Sixth Assessment Report of the Intergovernmental Panel on Climate Change*, Cambridge University Press, 553–672.

Lee, W.-L., and H.-C. Liang, 2020a: AS-RCEC TaiESM1.0 model output prepared for CMIP6 CMIP historical. https://doi.org/10.22033/ESGF/CMIP6.9755.

——, and ——, 2020b: AS-RCEC TaiESM1.0 model output prepared for CMIP6 ScenarioMIP ssp585. https://doi.org/10.22033/ESGF/CMIP6.9823.

Lovato, T., and D. Peano, 2020a: CMCC CMCC-CM2-SR5 model output prepared for CMIP6 CMIP historical. https://doi.org/10.22033/ESGF/CMIP6.3825.

——, and ——, 2020b: CMCC CMCC-CM2-SR5 model output prepared for CMIP6 ScenarioMIP ssp585. https://doi.org/10.22033/ESGF/CMIP6.3896.

——, ——, and M. Butenschön, 2021a: CMCC CMCC-ESM2 model output prepared for CMIP6 CMIP historical.

——, ——, and ——, 2021b: CMCC CMCC-ESM2 model output prepared for CMIP6 ScenarioMIP ssp585.

McGuffie, K., and A. Henderson-Sellers, 2014: *The Climate Modelling Primer*. John Wiley & Sons, 280 pp.

Meehl, G. A., R. Moss, K. E. Taylor, V. Eyring, R. J. Stouffer, S. Bony, and B. Stevens, 2014: Climate model intercomparisons: Preparing for the next phase. *Eos, Trans. Amer. Geophys. Union*, **95**, 77–78, https://doi.org/10.1002/2014EO090001.

NASA Goddard Institute for Space Studies (NASA/GISS), 2018: NASA-GISS GISS-E2.1G

model output prepared for CMIP6 CMIP historical. https://doi.org/10.22033/ESGF/CMIP6.7127.

——, 2019a: NASA-GISS GISS-E2-2-G model output prepared for CMIP6 CMIP historical.

——, 2019b: NASA-GISS GISS-E2.1H model output prepared for CMIP6 CMIP historical.

——, 2020a: NASA-GISS GISS-E2.1G model output prepared for CMIP6 ScenarioMIP ssp585. https://doi.org/10.22033/ESGF/CMIP6.7460.

——, 2020b: NASA-GISS GISS-E2.1H model output prepared for CMIP6 ScenarioMIP ssp585.

——, 2021: NASA-GISS GISS-E2-2-G model output prepared for CMIP6 ScenarioMIP ssp585.

O'Neill, B. C., and Coauthors, 2016: The scenario model intercomparison project (ScenarioMIP) for CMIP6. *Geosci Model Dev.*, **9**, 3461–3482.

Raäisaänen, J., 2007: How reliable are climate models? *Tellus A: Dyn. Meteor. Oceanogr.*, **59**, 2-29.

Rafferty, M. D., and Westermann E. J., 2023: Missouri. Encyclopedia Britannica, Accessed 18 April 2023, https://www.britannica.com/place/Missouri-state.

Ridley, J., M. Menary, T. Kuhlbrodt, M. Andrews, and T. Andrews, 2019a: MOHC HadGEM3-GC31-LL model output prepared for CMIP6 CMIP historical. https://doi.org/10.22033/ESGF/CMIP6.6109.

——, ——, ——, ——, and ——, 2019b: MOHC HadGEM3-GC31-MM model output prepared for CMIP6 CMIP historical.

Schneider, S. H., 1989: The greenhouse effect: science and policy. *Sci*, **243**, 771–781.

Schupfner, M., and Coauthors, 2019: DKRZ MPI-ESM1.2-HR model output prepared for CMIP6 ScenarioMIP ssp585.

Seferian, R., 2018: CNRM-CERFACS CNRM-ESM2-1 model output prepared for CMIP6 CMIP historical. https://doi.org/10.22033/ESGF/CMIP6.4068.

Seland, Ø., and Coauthors, 2019a: NCC NorESM2-LM model output prepared for CMIP6 CMIP historical. https://doi.org/10.22033/ESGF/CMIP6.8036.

——, and Coauthors, 2019b: NCC NorESM2-LM model output prepared for CMIP6 ScenarioMIP ssp585. https://doi.org/10.22033/ESGF/CMIP6.8319.

Semmler, T., and Coauthors, 2018: AWI AWI-CM1.1MR model output prepared for CMIP6 CMIP historical.

——, and Coauthors, 2019: AWI AWI-CM1.1MR model output prepared for CMIP6 ScenarioMIP ssp585.

Seneviratne, S. I., and Coauthors, 2021: Weather and climate extreme events in a changing climate. *Climate Change 2021: The Physical Science Basis. Contribution of Working Group I to the Sixth Assessment Report of the Intergovernmental Panel on Climate Change*, 1513–1766, https://doi.org/10.1017/9781009157896.013.

Shiogama, H., M. Abe, and H. Tatebe, 2019: MIROC MIROC6 model output prepared for CMIP6 ScenarioMIP ssp585. https://doi.org/10.22033/ESGF/CMIP6.5771.

Song, Z., F. Qiao, Y. Bao, Q. Shu, Y. Song, and X. Yang, 2019a: FIO-QLNM FIO-ESM2.0 model output prepared for CMIP6 CMIP historical. https://doi.org/10.22033/ESGF/CMIP6.9199.

——, ——, ——, ——, ——, and ——, 2019b: FIO-QLNM FIO-ESM2.0 model output prepared for CMIP6 ScenarioMIP ssp585. https://doi.org/10.22033/ESGF/CMIP6.9214.

Stouffer, R., 2019a: UA MCM-UA-1-0 model output prepared for CMIP6 CMIP historical. https://doi.org/10.22033/ESGF/CMIP6.8888.

——, 2019b: UA MCM-UA-1-0 model output prepared for CMIP6 ScenarioMIP ssp585. https://doi.org/10.22033/ESGF/CMIP6.13901.

Swart, N. C., and Coauthors, 2019a: CCCma CanESM5 model output prepared for CMIP6 CMIP historical. https://doi.org/10.22033/ESGF/CMIP6.3610.

——, and Coauthors, 2019b: CCCma CanESM5 model output prepared for CMIP6 ScenarioMIP ssp585. https://doi.org/10.22033/ESGF/CMIP6.3696.

Tachiiri, K., and Coauthors, 2019: MIROC MIROC-ES2L model output prepared for CMIP6 ScenarioMIP ssp585.

Tang, Y., S. Rumbold, R. Ellis, D. Kelley, J. Mulcahy, A. Sellar, J. Walton, and C. Jones, 2019: MOHC UKESM1.0-LL model output prepared for CMIP6 CMIP historical. https://doi.org/10.22033/ESGF/CMIP6.6113.

Tatebe, H., and M. Watanabe, 2018: MIROC MIROC6 model output prepared for CMIP6 CMIP historical. https://doi.org/10.22033/ESGF/CMIP6.5603.

Voldoire, A., 2018: CMIP6 simulations of the CNRM-CERFACS based on CNRM-CM6-1 model for CMIP experiment historical.

——, 2019a: CNRM-CERFACS CNRM-CM6-1 model output prepared for CMIP6 ScenarioMIP ssp585.

——, 2019b: CNRM-CERFACS CNRM-CM6-1-HR model output prepared for CMIP6 CMIP historical.

——, 2019c: CNRM-CERFACS CNRM-CM6-1-HR model output prepared for CMIP6

ScenarioMIP ssp585.

——, 2019d: CNRM-CERFACS CNRM-ESM2-1 model output prepared for CMIP6 ScenarioMIP ssp585. https://doi.org/10.22033/ESGF/CMIP6.4226.

Volodin, E., and Coauthors, 2019a: INM INM-CM4-8 model output prepared for CMIP6 CMIP historical. https://doi.org/10.22033/ESGF/CMIP6.5069.

——, and Coauthors, 2019b: INM INM-CM4-8 model output prepared for CMIP6 ScenarioMIP ssp585. https://doi.org/10.22033/ESGF/CMIP6.12337.

——, and Coauthors, 2019c: INM INM-CM5-0 model output prepared for CMIP6 CMIP historical.

——, and Coauthors, 2019d: INM INM-CM5-0 model output prepared for CMIP6 ScenarioMIP ssp585.

Wieners, K.-H., and Coauthors, 2019a: MPI-M MPI-ESM1.2-LR model output prepared for CMIP6 CMIP historical. https://doi.org/10.22033/ESGF/CMIP6.6595.

——, and Coauthors, 2019b: MPI-M MPI-ESM1.2-LR model output prepared for CMIP6 ScenarioMIP ssp585. https://doi.org/10.22033/ESGF/CMIP6.6705.

Wu, T., and Coauthors, 2018: BCC BCC-CSM2MR model output prepared for CMIP6 CMIP historical. https://doi.org/10.22033/ESGF/CMIP6.2948.

Xin, X., and Coauthors, 2019: BCC BCC-CSM2MR model output prepared for CMIP6 ScenarioMIP ssp585. https://doi.org/10.22033/ESGF/CMIP6.3050.

Yu, Y., 2019a: CAS FGOALS-f3-L model output prepared for CMIP6 CMIP historical. https://doi.org/10.22033/ESGF/CMIP6.3355.

——, 2019b: CAS FGOALS-f3-L model output prepared for CMIP6 ScenarioMIP ssp585. https://doi.org/10.22033/ESGF/CMIP6.3502.

Yukimoto, S., and Coauthors, 2019a: MRI MRI-ESM2.0 model output prepared for CMIP6 CMIP historical. https://doi.org/10.22033/ESGF/CMIP6.6842.

——, and Coauthors, 2019b: MRI MRI-ESM2.0 model output prepared for CMIP6 ScenarioMIP ssp585. https://doi.org/10.22033/ESGF/CMIP6.6929.

Zhang, X., L. Alexander, G. C. Hegerl, P. Jones, A. K. Tank, T. C. Peterson, B. Trewin, and F. W. Zwiers, 2011: Indices for monitoring changes in extremes based on daily temperature and precipitation data. *Wiley Interdiscp. Rev.: Climate Change*, **2**, 851–870.

Ziehn, T., and Coauthors, 2019a: CSIRO ACCESS-ESM1.5 model output prepared for CMIP6 CMIP historical. https://doi.org/10.22033/ESGF/CMIP6.4272.

——, and Coauthors, 2019b: CSIRO ACCESS-ESM1.5 model output prepared for CMIP6 ScenarioMIP ssp585. https://doi.org/10.22033/ESGF/CMIP6.4333.